Quantifying the Contributions of Aerosol and Snow-produced $ClNO_2$ through Observations and 1-D Modeling

Daun Jeong[1,a], Stephen M. McNamara[1], Qianjie Chen[1,b], Jessica Mirrielees[1], Jacinta Edebeli[1,2,c], Kathryn D. Kulju[1], Siyuan Wang[3,4], Laila Hayani[5], Rachel M. Kirpes[1], Nurun Nahar Lata[6], Swarup China[6], Jose D. Fuentes[7], Kerri A. Pratt[1,8*]

[1]Department of Chemistry, University of Michigan, Ann Arbor, MI 48109 USA
[2]Paul Scherrer Institut, Villigen 5232 Switzerland
[3]Chemical Sciences Laboratory, National Oceanic and Atmospheric Administration, Boulder, CO 80305 USA
[4]Cooperative Institute for Research in Environmental Sciences (CIRES), University of Colorado, Boulder, CO, 80309 USA
[5]Applied Physics Program, University of Michigan, Ann Arbor, MI 48109 USA
[6]Environmental Molecular Sciences Laboratory, Pacific Northwest National Laboratory, Richland, WA 99354
[7]Department of Meteorology and Atmospheric Science, Pennsylvania State University, University Park, PA 16802 USA
[8]Department of Earth and Environmental Sciences, University of Michigan, Ann Arbor, MI 48109 USA
[a]Currently at: Advanced Study Program, National Center for Atmospheric Research, Boulder, CO 80307 USA
[b]Currently at: Department of Civil and Environmental Engineering, The Hong Kong Polytechnic University, HongKong SAR, 999077 China
[c]Currently at: Center for Aviation, School of Engineering, Zurich University of Applied Science, Winterthur, 8401 Switzerland

*Corresponding Author: Kerri A. Pratt
Department of Chemistry, University of Michigan
930 N. University Ave.
Ann Arbor, MI 48109
prattka@umich.edu
(734) 763-2871

TOC

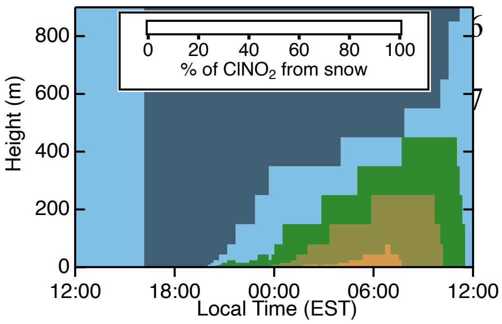
0
20
40
60
80
100
% of ClNO$_2$ from snow
Height (m)
800
600
400
200
0
12:00
18:00
00:00
06:00
12:00
Local Time (EST)

Abstract

Nitryl chloride ($ClNO_2$) is a radical reservoir that forms and accumulates in the nocturnal atmospheric boundary layer influenced by combustion emissions and chloride (e.g., sea salt and/or road salt). Upon sunrise, $ClNO_2$ rapidly photolyzes to generate highly reactive chlorine radicals ($Cl^{\cdot}$) that affect air quality by generating secondary air pollutants. Recent studies have shown road salt aerosols and the saline snowpack to be sources of $ClNO_2$ in the wintertime urban environment, yet the quantitative contributions of each chloride source are not known. In this study, we examine the vertically-resolved contributions of aerosol particles and the saline snowpack as sources of $ClNO_2$, using an observationally constrained snow-atmosphere coupled one-dimensional model applied to wintertime Kalamazoo, MI. Model simulations show that $ClNO_2$ emitted from the urban snowpack can be vertically transported throughout the entire atmospheric boundary layer, and can be a significant source of $ClNO_2$, contributing up to ~60 % of the $ClNO_2$ budget near the surface. Modeled snowpack $ClNO_2$ emission rates were 6 (±7) times higher than the observationally-derived emission rates, suggesting that not all snow chloride is available for reaction. $ClNO_2$ production from both aerosol particles and snow emissions are required to best simulate the observed surface-level $ClNO_2$. Using the bulk parameterization for $ClNO_2$ produced from particles significantly overestimated $ClNO_2$ observations, due to the assumption of equivalent dinitrogen pentoxide (N_2O_5) uptake and chloride availability for the entire particle population. In comparison, the chemically-resolved surface area-based parameterization slightly underestimated the observations, with uncertainties deriving from $ClNO_2$ production from residential wood burning particles.

1. Introduction

Nitryl chloride ($ClNO_2$) is a radical precursor that is formed and accumulates in the nocturnal stable atmospheric boundary layer due to its long lifetime at night ($\tau_{ClNO2} > 30$ h).[1,2] During the day, $ClNO_2$ rapidly photolyzes ($\tau_{ClNO2} \approx 30$ min, midday under summer-time mid-latitude conditions)[3] to generate chlorine radicals ($Cl^{\cdot}$) and $NO_2^{\cdot}$. $ClNO_2$ is formed through the heterogeneous reaction of gas-phase dinitrogen pentoxide (N_2O_5) on chloride (Cl^-) containing surfaces (R1).[4]

$$N_2O_{5(g)} + Cl^-_{(aq)} \xrightarrow{\gamma_{N2O5}} (2-\Phi_{ClNO2})\cdot HNO_{3(g)} + \Phi \cdot ClNO_{2(g)} \qquad \textbf{(R1)}$$

γ_{N2O5} is the reactive uptake coefficient of N_2O_5 on surfaces, and Φ_{ClNO2} is the branching ratio (yield) to produce gas phase $ClNO_2$. N_2O_5 is produced from the reaction of nitrogen dioxide ($NO_2^{\cdot}$) and the nitrate radical ($NO_3^{\cdot}$). N_2O_5 formation is enhanced at night, compared to daytime, when the lifetime of $NO_3^{\cdot}$ is short ($\tau_{NO3} < 5$ s), and N_2O_5 accumulates at night, with photolysis occurring upon sunrise. This is a reversible reaction in thermal equilibrium that favors N_2O_5 at lower temperatures, enabling greater accumulation during winter.[5]

$ClNO_2$ and its subsequent production of highly reactive Cl radicals influences tropospheric oxidation capacity by affecting the lifetime and chemistry of NO_x,[6] volatile organic compounds (VOCs),[7] mercury,[8] dimethyl sulfide,[9] and production of pollutants including ozone and secondary aerosols.[10,11] For instance, reactivity of Cl with alkanes can be up to two orders of magnitude higher than that of the hydroxyl radical ($^{\cdot}OH$),[12] which is the main oxidant in the troposphere.[13] Chemical transport models show that including heterogeneous formation of $ClNO_2$ from sea salt aerosols and biomass burning in the model framework can result in significant increases in modeled tropospheric O_3, especially during wintertime.[14–17]

Field observations show that $ClNO_2$ is ubiquitous in the boundary layer in both coastal[18–20] and inland regions.[21–28] Enhanced levels of $ClNO_2$ are attributed to air masses affected by sea salt aerosols,[19,23,29] biomass burning,[30] and coal burning activities,[26,31,32] with playa dust also found to be a $ClNO_2$ source.[33,34] While understudied, road salt can also be a significant source of chloride in the aerosol phase, as well as the urban snowpack.[27,35–40] Large amounts of road salts are used globally in wintertime environments for deicing purposes. In 2019, ~18 million tons of road salt was used in the U.S.[41] Road salts, which are mostly sodium chloride (NaCl),[42] are deposited on icy roadways and mechanically aerosolized by vehicular traffic.[43–46] Mielke et al.[47] reported enhanced $ClNO_2$ production following road salt application during snowfall in Calgary, Alberta, Canada. Similarly, McNamara et al.[35] reported up to ~220 parts per trillion (ppt) of $ClNO_2$, 12 m above the urban snowpack in Ann Arbor, Michigan, where they identified fresh and aged road salt aerosols. In Kalamazoo, Michigan, a maximum of ~ 90 ppt of $ClNO_2$ was observed at 1.5 m over snow-covered ground.[28]

The snowpack consists of interstitial air and snow grains with brine patches containing solutes excluded from the ice.[48] Therefore, snowpack is a highly porous media that serves as a unique matrix for multiphase reactions.[49–52] Laboratory[53–56] and field observations[57–60] demonstrate that snowpack reactions facilitate production of molecular halogen gases (Br_2, Cl_2, I_2, BrCl). Physical loss of N_2O_5 on surfaces can also be enhanced in the presence of ice/snow[61] and has been shown to be a significant (up to 25 %) chemical loss mechanism in the polluted wintertime boundary layer.[62,63] McNamara et al. showed that the reaction of N_2O_5 on saline snow produced $ClNO_2$. $ClNO_2$ fluxes derived from *in situ* measurements were reported during the winter in Kalamazoo, MI, where the fluxes on average were positive (emission) over snow compared to negative (deposition) over bare ground.[27] During the entire study, $ClNO_2$ was enhanced during periods with snowfall and snow-covered ground.[28] However, the contributions of $ClNO_2$ production from the saline snowpack compared to aerosols is not known.

Here we employ a one-dimensional (1D) model with a coupled snow-atmosphere framework that is required to quantify the vertically-resolved contributions of aerosols and the snowpack to boundary layer $ClNO_2$. Previous snow and atmospheric boundary layer-coupled 1D models, developed by Toyota et al.[64,65] and Thomas et al.,[66,67] implemented snow chemistry modules to represent multiphase halogen recycling mechanisms in the Arctic boundary layer. In those studies, the snow module embedded 1D model simulations were able to explain the snowpack-initiated radical chemistry and ozone depletion events in the Arctic boundary layer. A recent study by Wang et al.[40] implemented a similar chemical and physical framework for the midlatitude wintertime inland urban environment. By constraining the model with observations from Ann Arbor, Michigan, Wang et al.[40] simulated significant deposition of N_2O_5 and temperature-dependent emission of $ClNO_2$ from the urban snowpack. However, a comparison of $ClNO_2$ fluxes from the snowpack between observations[27] and model simulations has not been reported.

Significant challenges also remain in the simulation of $ClNO_2$ from aerosol particles.[68,69] Laboratory studies have shown that particle γ_{N2O5} and Φ_{ClNO2} are dependent on aerosol composition, including sulfate,[70,71] chloride,[72,73] nitrate,[72,74] and organic[75–80] content, as well as aerosol water content[74,81] that also depends on relative humidity and temperature.[82] However, discrepancies exist between these bulk-derived parameters and field-derived values.[25,30,32,68,83–87] Note that γ_{N2O5} and Φ_{ClNO2} for snow/ice are even less known with only limited laboratory studies[53,72,88,89] available that show these parameters vary with temperature and halide content at the ice surface. In order to estimate the production of $ClNO_2$ in model simulations, the most commonly used parameterization assumes a homogenous distribution of chemical composition across the aerosol population.[72,90] A recent study by McNamara et al.[35] in the wintertime inland environment showed that only road salt aerosol contained significant levels of chloride, and these aerosols comprised ~20 % of the total particulate surface area concentration. By weighting γ_{N2O5} and Φ_{ClNO2} by the surface area contributions of the different individual particle source types (e.g., road salt, biomass burning, soot, dust) through their new parametrization, McNamara et al.[35] were able to reconcile the measured $ClNO_2$. In the current work, we test this new parametrization[35] with another observational dataset to examine its effectiveness compared to the traditional bulk approach.[72]

In this study, we investigate the vertically-resolved contributions of $ClNO_2$ emissions from an urban snowpack in Kalamazoo, MI during the SNow and Atmospheric Chemistry in Kalamazoo (SNACK) campaign using the 1D atmospheric boundary layer model coupled to a snow module.[27,40] The ambient gas, particle, and snow measurements, reported by Kulju et al.[28] and observationally derived $ClNO_2$ and N_2O_5 fluxes, reported by McNamara et al.[27], are constrained in the 1D model. To evaluate the coupled snow module, the modeled $ClNO_2$ flux is compared to the measurement-derived fluxes reported by McNamara et al.[27] In addition, $ClNO_2$ production from aerosol particles is investigated by comparing the traditional bulk parametrization[72] with the new chemically-resolved, surface area-based (single-particle) parametrization.[35] The vertically-resolved relative contributions of the snowpack and aerosols as sources of $ClNO_2$ are quantified.

2. Methods

The SNACK campaign was carried out in Kalamazoo, MI (longitude: 85.6105° W latitude: 42.2784° N) in the winter (Jan. 12 to Feb. 24) of 2018.[28] We focus our modeling study here on two case periods: 1) the night of Jan. 31 (Jan. 31 12:00 – Feb. 1 12:00 Eastern Standard Time (EST)) representing the bare ground case and 2) the night of Jan 30 (Jan. 30 12:00 – Jan. 31 12:00 EST) representing the snow-covered ground case. Photographs of the site on each case day are shown in **Figure 1**. The bare ground case corresponds to no snow on the land but areas covered by grass and dirt and pavement roads. **Section 2.1** summarizes the observations used in this study, **Section 2.2** describes the 1D model framework, and **Section 2.3** describes the parameterizations of N_2O_5 uptake and $ClNO_2$ yield on aerosols and snow grains used in the model simulations. Additional details can be found in the supporting information.

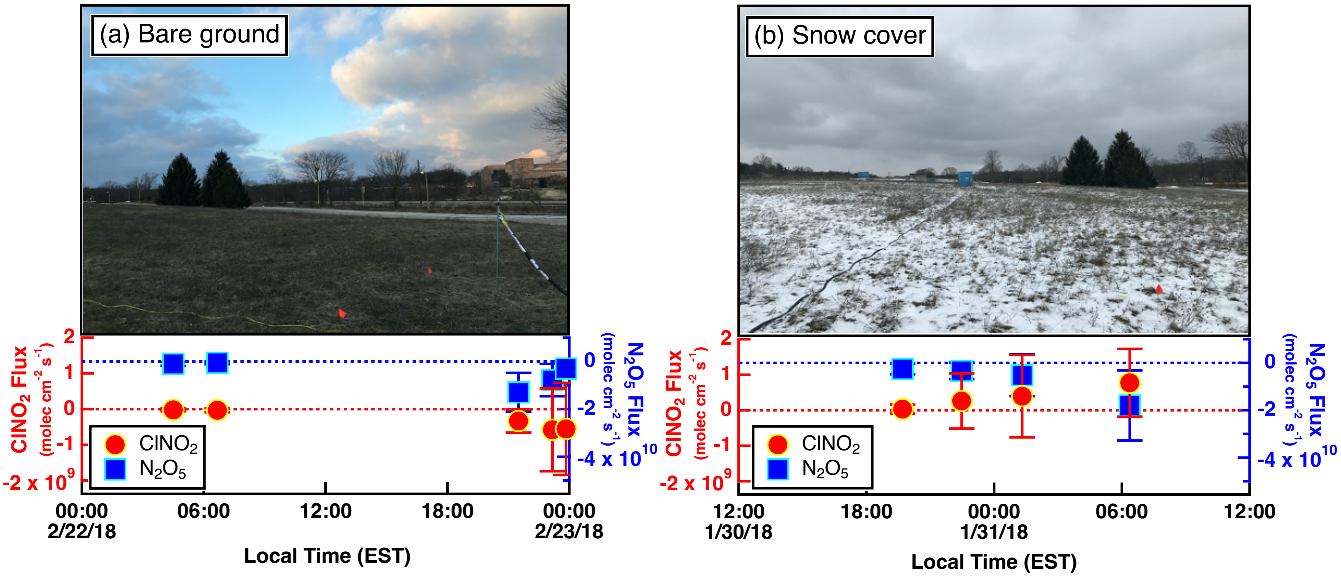

Figure 1 $ClNO_2$ and N_2O_5 fluxes derived from vertical profile measurements during the two representative (a) bare ground and (b) snow cover days, as reported by McNamara et al.[27] Photos of the field site on the corresponding days (Bare ground: Jan 31; Snow cover: Jan 30) are shown. Measurement uncertainties are shown as error bars, and dashed lines show zero values for N_2O_5 (blue) and $ClNO_2$ (red) fluxes for context. Flux data from Feb 22 are used in our model study as vertical profile measurements were not carried out on the night of Jan 31, which we define as the bare ground case day for the subsequent modeling.

2.1.Measurements and sampling during the SNACK campaign

The field site was situated ~ 90 m from a heavy traffic road, where road salt was routinely applied in the winter. A comprehensive suite of gas phase and particle phase instruments were housed in a research trailer next to a field on the Western Michigan University (WMU) campus. Ambient $ClNO_2$ and N_2O_5 were measured at 1.5 m above ground with a chemical ionization mass spectrometer (CIMS, THS instruments)[91] using iodide water clusters ($I\cdot(H_2O)^-$) as the reagent ion to form iodide adduct with $ClNO_2$ ($IClNO_2^-$, *m/z* 208 and 210) and N_2O_5 ($IN_2O_5^-$, m/z 235).[92] Details of the CIMS measurements during the SNACK campaign can be found in McNamara et al.,[27] Kulju et al.,[28] and in the supporting information (S1).

Ambient O_3 was measured with a dual beam ozone monitor (model 205, 2B Technologies, limit of detection (LOD) 2 parts per billion, ppb) on the CIMS inlet. Gas-phase hydrochloric acid (HCl) and $PM_{2.5}$ (particles <2.5 μm in diameter) Cl^- (LOD 0.004 $\mu g\ m^{-3}$) and NO_3^- (LOD 0.05 $\mu g\ m^{-3}$) were sampled at 3 h resolution and analyzed with an ambient ion monitor-ion chromatography (AIM-IC) system (model 9000D, URG Corp., Chapel Hill, NC) with a modified inlet, described by Markovic et al.,[93,94] at 1.8 m above ground. Temporal variation of gas-phase HCl and $PM_{2.5}$ Cl^- and NO_3^- for the two case days are shown in **Figures S1** and **S2**, respectively. More details of the AIM-IC sampling method during the campaign are described by Chen et al.[95] Size-resolved number concentrations of atmospheric aerosols were measured at ~3 m with a scanning mobility particle sizer (SMPS, model 3082, TSI Inc.) for 14 – 736 nm mobility diameters and with an aerodynamic particle sizer (APS, model 3321, TSI Inc.) for 0.542– 20 μm aerodynamic diameters (d_a). Total surface area of particles with d_a between 20 nm and 20 μm were derived by converting mobility diameters to aerodynamic diameters assuming a shape factor of 1 and density of 1.5 $g\ cm^{-3}$.[96] Temporal variations of the particle number densities and total surface areas for the two case days are shown in **Figure S3,** and the 24 h averaged size distribution is shown in **Figure S4**.

Size-resolved individual atmospheric particle composition was measured for the two case days. Atmospheric particles were collected on transmission electron microscopy (TEM) grids (Ted

Pella, Inc.) using a micro-orifice uniform deposit impactor (MOUDI, model 110R, MSP Corp). The MOUDI sampled air at 11 L min^{-1}, which was diluted with 19 L min^{-1} of particle-free (HEPA capsule, Pall Laboratory) air, for a total flow of 30 L min^{-1}. On Jan 30 19:29-Jan 31 6:50 EST (snow cover case), particles were collected on the 0.10-0.18 µm d_a and 0.32-0.56 µm d_a stages. On Jan 31 17:18-Feb 1 8:00 EST (bare ground case), particles were collected on 0.18-0.32 µm, 0.32 – 0.56 µm, and 1.0-1.8 µm d_a stages. The collected samples were stored in the laboratory in air-tight clean plastic containers until they were analyzed with computer-controlled scanning electron microscopy with energy dispersive X-ray spectroscopy (CCSEM-EDX).[38] In total, 22,223 individual particles were analyzed for the case day samples. Representative SEM images and EDX spectra for the individual particle types observed are shown in **Figure S5,** and additional details of the CCSEM-EDX analysis and results are described in the supporting information (**S5**).

Snow samples were collected from the top 2 cm of the surface of the snowpack in various locations near the trailer as shown in McNamara et al.[27] Four snow samples, collected between 20:00 of January 30 to 7:00 of January 31, were used in this study. The collected snow was put in sterile Whirl-pak bags, kept in the freezer (-20 to -30 ^{o}C), and thawed prior to analysis. Sodium, chloride, and nitrate content in the melted snow samples were analyzed with ion chromatography (IC) using a Dionex ICS-1100 for cations and an ICS-2100 for anions. The pH of the melted snow was measured with a pH meter (model AP110, Fisher Scientific). The density of the snow was measured with an aluminum density gauge (model Scientist200, Brooks-Range). Snow density was measured for nine snow samples collected between February 5 and 14. The average snow density of 0.36±0.06 g cm^{-3} was used in this study, because there was little variability and since the snow on the night of January 30 was not deep enough to use the snow density gauge. A summary of the observed snow parameters used in the model are shown in **Table S2**.

Ambient temperature (270 ± 5 K) (**Figure S7**) and three-dimensional wind speeds and wind directions (**Figure S8**) were measured with the sonic anemometer (model CSAT3, Campbell Scientific Inc.) at ~1.4 m above ground level to estimate the friction velocity (u^*) and the atmospheric eddy diffusivity (K_z). Ultraviolet solar radiation ($0.295 < \lambda < 0.385$ μm) was measured with a UV radiometer (model TUVR, Eppley Laboratory). Relative humidity (RH) was measured at the Kalamazoo Battle Creek International Airport (KAZO), which is ~ 7 km from the field site. The averaged RH values were 66 (±9) % for the bare ground case day (Jan. 31 12:00 EST – Feb. 1 12:00) and 61 (±7) % for the snow cover day (Jan. 30 12:00 – Jan. 31 12:00). Therefore, for all the model runs, a RH of 65 % was used.

2.2. 1-Dimensional model description

A 1D atmospheric model with a coupled snow module, developed by Wang et al.,[40] was used to simulate the temporal and vertical profiles of $ClNO_2$ for the two case study scenarios (bare ground and snow cover). A simple schematic of the model framework is illustrated in **Figure S9**. The 1D model[40] is an IGOR (WaveMetrics, Inc., Lake Oswego, OR) based framework with a similar concept of air-snow interactions as described by Thomas et al.[66] and Toyota et al.[64] Brief descriptions of the parameterizations of N_2O_5 uptake and $ClNO_2$ yield values and snow module are described in Sections 2.2.1 and 2.2.2, respectively. For all model simulations, both bare ground and snow cases, the N_2O_5 surface deposition velocity was constrained to the measurement-derived averaged value (0.5 cm s^{-1}) reported by McNamara et al.[27] as it was shown to not be statistically different between snow covered and bare ground surfaces. Additional details of the model and how it is constrained can be found in Wang et al.[40] and in the supporting documents (**S2** and **S3**).

$PM_{2.5}$ chloride and nitrate, ozone, and N_2O_5 levels measured during the campaign were constrained diurnally at every model time step (10 min) at the model height of 1 m. Total particulate surface area concentrations from observations were constrained to be the same for all model layers. Other trace gases including NO_2 and VOCs were taken from nearby air quality observation stations or from previous literature and are summarized in **Table S1**. To enable proper model spin-up, we report the simulation results of the third model day. Photolysis rate constants (J) of gas-phase compounds were calculated using the clear sky Tropospheric Ultraviolet and Visible (TUV) model[97] and scaled to the solar radiation measured during the two case days.

2.2.1. N_2O_5 uptake and $ClNO_2$ yield parameterization for aerosols

We used two types of parameterizations of N_2O_5 uptake ($\gamma_{N2O5,p}$) and $ClNO_2$ yield ($\Phi_{ClNO2,p}$) by aerosols. The first is the commonly used bulk parameterization from Bertram and Thornton,[72] which assumes homogeneous composition of the aerosol population through calculations using bulk aerosol mass concentrations. Time-resolved $PM_{2.5}$ NO_3^- and Cl^-, measured by AIM-IC during the campaign, were used for the bulk parameterization calculations. More details can be found in the supporting information (**S4**). The second is the new chemically-resolved, surface area-based ('single-particle') parameterization method,[35] which uses individual particle composition obtained from the CCSEM-EDX measurements. The particles collected on the nights of January 30 (Jan. 30 19:29 – Jan. 31 6:50) and on the night of January 31 (Jan. 31 17:18 – Feb. 1 8:00) were grouped into four categories: organic (biomass burning), soot, aged road salt, and mineral dust particles. The size-resolved number fractions of each particle type, determined by CCSEM-EDX analysis, are shown in **Figure S6,** and more details of the analysis are in the supporting information (**S5**). $\gamma_{N2O5,p}$ and $\Phi_{ClNO2,p}$ corresponding to each particle type were based on proxies from previous laboratory studies (**Table S3)** and then weighted by the surface area concentration contribution of each particle type. For particle size bins below and above which single-particle composition was measured (Figure S6), the particles were assumed to have the same particle composition as the lowest and largest bin sizes, respectively. The surface area of these particles accounted for 6.5 % (5.9 % for smaller and 0.6 % for higher particles) for the bare ground case and 15.4 % (4.7 % for smaller and 10.7 % for higher particles) for the snow cover case day.

2.2.2 Model snow $ClNO_2$ production

For the snow case, snowpack $ClNO_2$ emissions were incorporated in two ways: 1) constraining by measurement-derived fluxes[27] and 2) calculating emissions within the snow module.[40] For model simulations constrained by measurement-derived $ClNO_2$ fluxes, the time-dependent $ClNO_2$ emission rate from the snow was constrained based on the $ClNO_2$ fluxes derived from gradient profile measurements that occurred every 3-5 hours for 30- 58 mins for each profile during the night of the snow cover day (Jan. 30 12:00 – Jan. 31 12:00).[27] Fluxes were interpolated for periods between profiles. Snowpack $ClNO_2$ emissions were assumed to be zero during the day when the model was constrained by measurement-derived $ClNO_2$ fluxes in the model. Sensitivity of the simulations to the upper and lower bounds of the uncertainties in the measurement-derived $ClNO_2$ fluxes were carried out by constraining the model accordingly. For the lower bound, the snowpack $ClNO_2$ emission rate was set to zero as the uncertainties in the measurement-derived $ClNO_2$ fluxes resulted in deposition of $ClNO_2$.

As described by Wang et al.,[40] the snowpack, consisting of snow grains and interstitial air, is the bottom layer of the model framework (**Figure S9**). The snow parameters were constrained in the model based on measurements described in **Section 2.1** and are summarized in **Table S2**. The snowpack depth at the field site during the snow case day was variable (< 5 cm) but was often close to ~ 1 cm, to which the snow depth value was constrained in the model snow module (**Table S2**). The snow grain diameter and density were constrained in the snow module based on our best measurement estimates as outlined in Section 2.1. Snow grains were assumed to be spherical with a liquid brine layer on the surface, following Thomas et al.[66] The liquid brine layer fraction (f_{brine}) was calculated based on Cho et al.[98] using snow meltwater Na^+ and Cl^- concentrations. All snow grains in the model snowpack are assumed to be available for reaction. Heterogeneous uptake of N_2O_5 on snow grains was derived based on a resistor analogue model following Wang et al.[40] The snow $ClNO_2$ yield was calculated based on Bertram and Thornton[72] in the same manner as for aerosol particles (Section 2.2.1). Additional details can be found in the supporting information (**S4**).

3. Results and Discussion

3.1. N_2O_5 and $ClNO_2$ observations during the bare ground and snow cover case studies.

N_2O_5 and $ClNO_2$ observations for the full SNACK campaign were previously reported by Kulju et al.[28] Over the full campaign, N_2O_5 mole ratios were not statistically significantly different between snow-covered and bare ground periods.[28] In contrast, on average over the full campaign, $ClNO_2$ mole ratios were higher over snow-covered compared to bare ground due to snowpack $ClNO_2$ production.[28]Here we focus this modeling study on two case studies – the nights of Jan 31 and Jan 30 – chosen to represent bare ground and snow cover periods, respectively (**Figure 1**). The ratio of snowmelt Na^+ to Cl^- (**Table S2**) was close to 1 showing that the snowpack Cl^- was mostly from road salt. Measurements of O_3, N_2O_5, and $ClNO_2$ at 1.5 m above ground, as well as calculated $ClNO_2$ photolysis rate coefficients, are shown in **Figure 2** for the two case days, with meteorological data shown in **Figures 2** and **S8**. McNamara et al.[27] quantified $ClNO_2$ and N_2O_5 fluxes over both bare ground and snow cover, enabling investigation of the roles of these surface fluxes in the current modeling study (**Figure 1**).

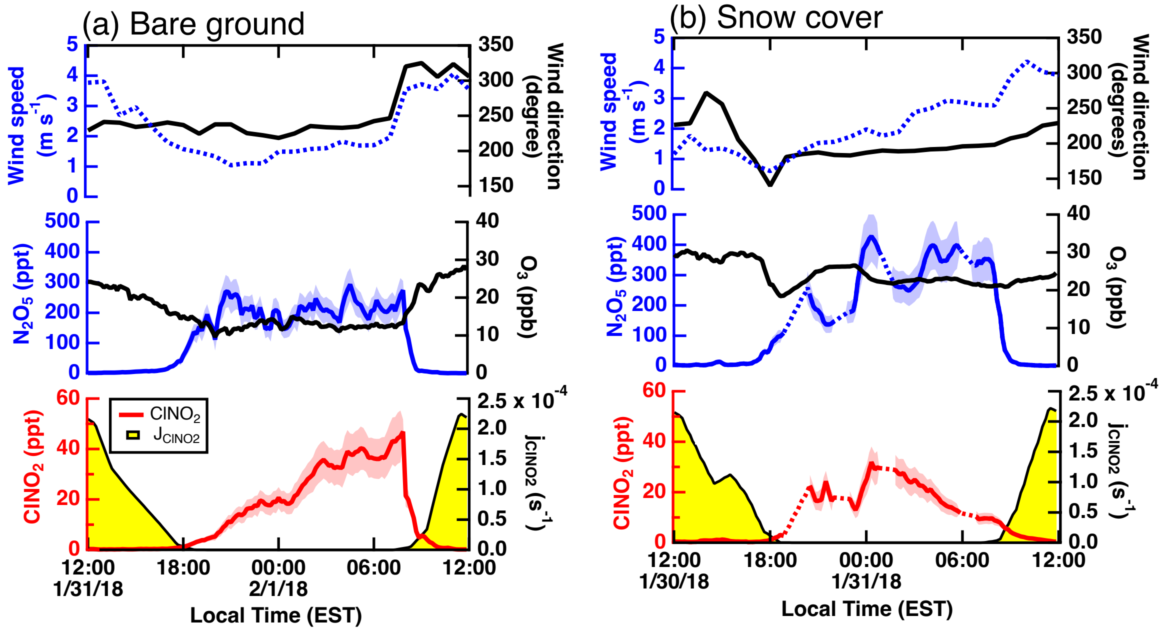

Figure 2 One h averaged wind directions and 10 min averaged diel variations of O_3, N_2O_5, $ClNO_2$, and $ClNO_2$ photolysis rate coefficients (J_{ClNO2}) during the (a) bare ground and (b) snow cover case days. Time-dependent measurement uncertainties of N_2O_5 and $ClNO_2$ are shown as shades. Gaps in ambient data in Fig. 2b (dashed lines showing interpolation) occurred when vertical profile measurements were carried out.

The bare ground case night (Jan. 31 – Feb. 1) had stable atmospheric conditions with constant wind direction and speed (average of 1.4 ± 0.3 m s^{-1}) resulting in a friction velocity of 0.1 – 0.2 m s^{-1} and eddy diffusivity of ~0.05 m^2 s^{-1} (**Figure S8a**). During the night, average O_3 levels were 12 ± 1 ppb (range of 10 to 15 ppb). This shows that ozone was not completely titrated by NO from local vehicular emissions.[99–101] N_2O_5 levels showed stable sustained levels of 150 - 250 ppt, while $ClNO_2$ steadily increased through the night to ~ 50 ppt, then started declining upon sunrise (7:56 am local time) (**Figure 2a**). The lifetime of $ClNO_2$ in the early morning (9:00 – 10:00 local time, EST) was calculated to be ~6 h, and ~80 min at midday (11:00 – 13:00).

Vertical profile measurements to calculate $ClNO_2$ fluxes were not carried out on the night of the bare ground case (Jan. 31 – Feb. 1). Therefore, for this modeling study, $ClNO_2$ fluxes from vertical profiles measured on the bare ground night of Feb 22-23 are used (Figure 1). The friction velocity during the night of Feb 22 was an average of 0.18 ± 0.03 m s^{-1} and during the night of Jan 31 was 0.3 ± 0.1 m s^{-1}. **Figure 1a** shows that the average $ClNO_2$ flux on Feb 22-23 was -3.0×10^{8} ($\pm 2.7\times10^{8}$) molec cm^{-2} s^{-1}, showing that there was net deposition of $ClNO_2$ to the surface. For context, the bare ground $ClNO_2$ flux averaged over the entire field study was -2.4×10^{8} ($\pm 2.3\times10^{8}$) molec cm^{-2} s^{-1}.[27] The calculated average $ClNO_2$ deposition velocity on the night of Feb. 22 was 0.5 ± 0.3 cm s^{-1}, which is not statistically different from the campaign averaged $ClNO_2$ deposition velocity, during bare ground days that showed negative $ClNO_2$ fluxes, of 0.2 ± 0.3 cm s^{-1} ($p=0.9$).[27] For N_2O_5, the flux was not statistically significantly different between the snow cover and bare ground nights, with a campaign average of -2.8×10^{9} ($\pm 0.9\times10^{9}$) molec cm^{-2} s^{-1}.[27]

During the snow cover case night, wind speeds were ~1.7 m s^{-1} prior to ~1:00 – 2:00 local time, and increased afterwards (**Figure 2**). Following this wind speed transition, the friction velocity was > 0.25 m s^{-1}, and eddy diffusivity were > 0.05 m^2 s^{-1} (**Figure S8b**). As a result, the snow cover case (**Figure 2b**) showed greater fluctuations in the trace gas levels compared to the bare ground case. During the night, O_3 showed an average of 23 ± 2 ppb (range 21 to 26 ppb). Nighttime N_2O_5 varied between 100 and 400 ppt. $ClNO_2$ reached a maximum of ~40 ppt at 1:00 – 2:00 and then steadily decreased for the remainder of the night. For the full SNACK field campaign, Kulju et al.[28] showed that nighttime $ClNO_2$ levels over snow covered ground were ~ 3 times higher on average compared to over bare ground. Nighttime $ClNO_2$ levels during the two case days, used in this study, averaged over 18:00 to 8:00 local time, were 24 ± 13 ppt for the bare ground case night and 17 ± 8 ppt for the snow cover night. However, when averaged from 18:00 to 1:00 local time (to account for the mixing event on the snow case night), averaged $ClNO_2$ was 17 ± 9 ppt for the snow cover night and 12 ± 7 ppt for the bare ground night, showing that the $ClNO_2$ levels over snow cover were indeed significantly higher ($p=0.017$). The increased atmospheric turbulence at around 1:00-2:00 corresponded to an air mass shift that resulted in decreases in both O_3 and N_2O_5 at ~1:00 (**Figure 2b**). Total particle (14 nm – 20 μm in diameter) surface area concentration (**Figure S3b**) and $PM_{2.5}$ chloride mass concentration (**Figure S2b)** also decreased at ~1:00. For the remainder of the night after ~ 3:00, N_2O_5 and $PM_{2.5}$ chloride remained approximately constant (350 ppt and 0.06 μg m^{-3}, respectively), while friction velocity continued to increase and $ClNO_2$ and particle surface area concentrations continued to decrease.

Four vertical profile measurements were carried out on the night of the snow case (Jan. 30-31) (**Figure 1(b)**). As reported by McNamara et al.,[27] the N_2O_5 deposition velocity averaged over the snow cover days throughout the entire study was 0.5 ± 0.2 cm s^{-1}, with the snow case night average being 1.0 ± 0.8 cm s^{-1}. On the snow case night, a positive $ClNO_2$ flux was calculated, with an average of 3.7×10^8 ($\pm 3.1\times10^8$) molec cm^{-2} s^{-1}, showing net emission from the snowpack. This result is in line with the campaign average $ClNO_2$ flux over snow of 3×10^7 ($\pm 14\times10^7$) molec cm^{-2} s^{-1}.[27]

3.2. Model overestimates observed snowpack $ClNO_2$ flux

Simulations of atmospheric $ClNO_2$ were carried out using a coupled atmosphere-snow 1D model.[40] To examine only snowpack-produced $ClNO_2$, $ClNO_2$ production from aerosols was turned off for the first model scenario. **Figure 3** shows the model results of the time-resolved vertical distribution of $ClNO_2$ when (a) the snow module was used to calculate $ClNO_2$ production, compared to when (b) the model was instead constrained by the observationally derived fluxes[27] (**Figure 1b**). The model simulated snowpack $ClNO_2$ flux averaged 1.6×10^9 ($\pm 0.6 \times 10^9$) molec cm^{-2} s^{-1}, with a range of $0.7 - 3.1 \times 10^9$ molec cm^{-2} s^{-1} during the snow cover case night, representing net emission of $ClNO_2$ from the snowpack (**Figure 3a**). This $ClNO_2$ snowpack flux is a factor of 6 (± 7) higher than what was derived from measurements (**Figure 3b**), as reported by McNamara et al.[27] As a result, the snow module simulated near-surface (1.4 m) $ClNO_2$ (**Figure 3a**) was on average 100 (± 25) ppt (range 50 – 135 ppt) at night; this corresponds to up to ~ 10 times (average 6 times) higher than the observations, representing a significant overestimate. In contrast, the simulations constrained with the observationally driven fluxes (**Figure 3b**) underestimated the observation mole ratios at 1.4 m until 2-3 am EST. For the remainder of the night, the measured $ClNO_2$ declined, as discussed in Sec. 3.1, and the flux-constrained model simulations overestimated the observations up to ~3 times. However, the uncertainties in the measurement-derived $ClNO_2$ fluxes resulted in a wide range of simulated $ClNO_2$ (near zero to ~100 ppt near the surface) (**Figure 3b**). Within this wide range of uncertainty in $ClNO_2$ fluxes, the observations were within the uncertainty of model simulations. However, this does not imply that the measured $ClNO_2$ could be solely explained by snow emissions. Rather, this result further shows that the model is sensitive to the snowpack $ClNO_2$ flux demonstrating its important and yet highly uncertain role in producing near-surface $ClNO_2$.

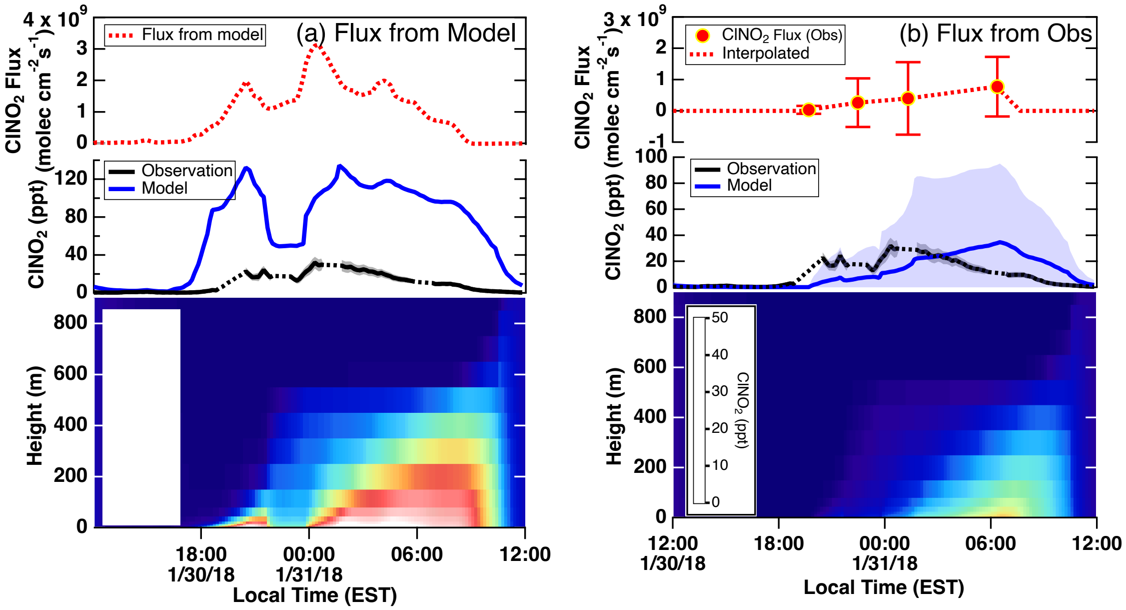

Figure 3 $ClNO_2$ model simulation results when (a) using the model snow module and (b) constraining the model with observationally derived $ClNO_2$ flux reported by McNamara et al. (2021) and also shown in Figure 1b. (*top*) Diel variation of model simulated and observationally derived $ClNO_2$ fluxes, which were interpolated (dashed line, flux set to zero between sunrise and sunset) and constrained in the model. Error bars are shown for measurement uncertainties. (*middle*) $ClNO_2$ measurements (black, uncertainty in shade) compared to model

resolved vertical profiles of model simulated $ClNO_2$.

The significant difference in the $ClNO_2$ fluxes calculated by the snow module and derived from observations shows that uncertainties remain in simulating snowpack production of trace gases. In this model[40] and following other snow models,[66,67] we assumed that spherical snow grains are entirely covered with brine and are available to react with N_2O_5 to release $ClNO_2$. This assumption means that all chloride measured in the snow melt is assumed to be at the snow grain surface in the brine.[40,98] However, this is unrealistic and an upper limit as additional unknown physical or chemical factors that limit the formation and subsequent transport within the snowpack may exist.[102] For example, within a likely non-spherical snow grain, chemical species are not homogeneously distributed, with spatial variation between brine patches, grain boundaries, and ice crystal surfaces, which is not currently represented in model frameworks.[102–104] Not all snow chloride is expected to be available for reaction to generate $ClNO_2$, and this is one of many uncertainties likely leading to the snow module overestimating the observed $ClNO_2$ in **Figure 3**.

An additional uncertainty is the N_2O_5 uptake and $ClNO_2$ yield values on snow grains, for which laboratory studies are lacking. A qualitative snow chamber study by McNamara et al.[27] exposed local snow to synthesized N_2O_5 during the SNACK campaign. The results showed that snowpack physical structure characteristics, which are influenced by temperature and the use of deicing materials, control the availability of snow Cl^- and reactive surface area. [27] In our modeling study, the snowpack temperature was assumed to be the same as the near-surface air, which is an upper limit that affects the calculated N_2O_5 uptake and $ClNO_2$ yield values and model simulated $ClNO_2$. [40] Due to latent heat of fusion for phase transition and radiational cooling, the snowpack temperature is likely lower than the overlying air since snow patches remained when the air temperature was above freezing in the early morning of Feb. 1 (**Figure S7**). This overestimated temperature in the model drives the snow grain brine fraction (f_{brine}) to be higher, which dilutes the chloride content and therefore results in lower yields. The snow f_{brine} was calculated to be 0.1 - 1 % during the night and reach 100 % in the early morning as the temperature constrained in the model increased to over the freezing point, set as 273 K (**Figure S7)**. Based on the fraction of the liquid brine layer and the resulting ion concentration of snow grains, $\gamma_{N2O5,s}$ ranged between 0.023-0.027, within the wide range (10^{-4} – 0.1) of $\gamma_{N2O5,}$ reported by laboratory and field studies on particles.[69] The calculated $\Phi_{ClNO2,s}$ was sensitive to temperature and ranged from 0.4 to 1 during the night and dropped to near zero when the snow f_{brine} was calculated to be 1 (i.e. complete snowmelt, which was not observed), leading to significant dilution of chloride. This is consistent with the previous discussion by Wang et al.,[40] in which the model calculated $\Phi_{ClNO2,s}$ was found to be highly sensitive to temperature. Further, both $\gamma_{N2O5,s}$ and $\Phi_{ClNO2,s}$ of snow grains are a function of chloride in the model.[40] The nitrate effect that can suppress $ClNO_2$ formation[72] is expected to be insignificant considering the low levels (29 ± 3 μM, ~15 times less than Cl^- or Na^+) measured from the snow samples collected on the snow case day.[27] Overall, further studies are needed to characterize the efficiency of $ClNO_2$ generation and release from the snowpack.[53]

As expected, **Figure 3** shows that simulated $ClNO_2$ levels were highest near the ground for the snowpack-produced $ClNO_2$ model scenarios. However, the model results also show that the snowpack-produced $ClNO_2$ was vertically transported throughout the nocturnal stable boundary layer, the depth of which was estimated to be ~ 450 m (**Figure S10b**). The drop in $ClNO_2$ mole ratios between 21:00 and 23:00 EST, observed in both in the model simulations and observations, is likely due to enhanced atmospheric mixing as evidenced by the increase in the vertical eddy diffusivity (**Figure S3b**) during this time period. The modeled $ClNO_2$ was confined to the nocturnal stable boundary layer with no significant levels in the residual layer aloft as the production from aerosol particles were turned off in the model and therefore the snow-covered ground was the only source of $ClNO_2$.

3.3. Single-particle (chemically-resolved surface area) parameterization improves $ClNO_2$ simulation

In this section, we compare ground level (1.4 m) $ClNO_2$ observations to model simulations with various scenarios of aerosol particles and/or snowpack as sources of $ClNO_2$ (**Figure 4**). As described in section 2.3, we use two parameterization methods for deriving $\gamma_{N2O5,p}$ and $\Phi_{ClNO2,p}$ in simulating $ClNO_2$ generation from aerosol particles: 1) bulk method[72] and 2) single-particle (chemically-resolved surface area) parameterization.[35] The bulk parameterization assumes that all particles have identical composition, while the single-particle parameterization is based on measurement-derived chemically resolved surface area concentrations. This new parameterization accounts for variations between particle types (e.g. soot vs. road salt) in N_2O_5 uptake and $ClNO_2$ production, enabling only a subset of aerosol particles to produce $ClNO_2$. For the single-particle method, calculated surface-area weighted $\gamma_{N2O5,p}$ and $\Phi_{ClNO2,p}$ values reported in the literature were applied for different particle types (**Table S3**). In **Figure 4**, model scenario 1 (Sc1) uses the bulk method[72] and scenario 2 (Sc2) uses the single-particle parameterization for $ClNO_2$ production.[35] For both scenarios (Sc1 and Sc2), snowpack $ClNO_2$ production was turned off in the model, and therefore aerosol particles were the only source of simulated $ClNO_2$. For scenario 3 (Sc3), $ClNO_2$ was produced from aerosols through the single particle method; in addition, the measured $ClNO_2$ surface flux (depositing over bare ground, Figure 4a, or emitting over snow cover, Figure 4b) was constrained.[27] Scenario 4 (Sc4) was similar to Sc3, with the $ClNO_2$ yield from particles increased by a factor of 3.

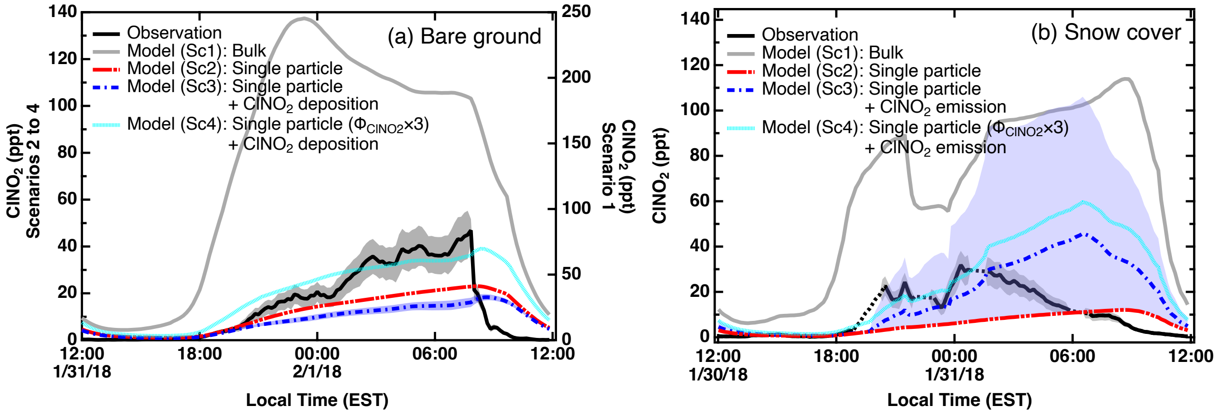

Figure 4 Comparison between measured and modeled $ClNO_2$ during (a) bare ground and (b) snow cover case days. Model results from the atmospheric layer corresponding to the measurement height (1.4 m) are shown. Scenario 1 (Sc1), scenario 2 (Sc2), and scenario 3 (Sc3) show modeled $ClNO_2$ using the particle bulk parameterization, single particle parameterization, and single particle parameterization with measured $ClNO_2$ emission/deposition constrained, respectively. Scenario 4 (Sc4) was similar to Sc3, with the $ClNO_2$ yield increased by three times. For observations (black), grey shades are uncertainties, and the black dashed line shows interpolated points from when vertical profile measurements were conducted. For S3, blue shades correspond to when the model is constrained with upper and lower bounds of deposition (a, bare ground) and emission (b, snow cover). Emissions during the snow case day were set to zero for the lower bound.

The results of the ground level $ClNO_2$ model simulations show that the bulk method (Sc1) overestimates the $ClNO_2$ levels, while the single-particle parameterization (Sc2) underestimates them (**Figure 4b**). For the bare ground case (**Figure 4a**), Sc1 overestimated $ClNO_2$ mole ratios by an average factor of 10 (range 4 - 27 times), while Sc2 underestimated on average by 40 %. For the snow cover case (**Figure 4b**), Sc1 overestimated by an average factor of 5 (range 2-11 times), while Sc2 underestimated on average by a factor of 3 (range 0.8 – 7). In the bulk parameterization, calculated $\gamma_{N2O5,p}$ and $\Phi_{ClNO2,p}$ are driven by particle liquid water content and measured particulate chloride and nitrate mass concentrations (**Figure S2**). The bulk method gives $\gamma_{N2O5,p}$ values ranging from 0.019 to 0.031 (average 0.0252 ± 0.004) and $\Phi_{ClNO2,p}$ values ranging from 0.815 to 0.983 (average 0.92 ± 0.07) for the bare ground case, and $\gamma_{N2O5,p}$ values ranging from 0.025 to 0.036 (average 0.029 ± 0.004) and $\Phi_{ClNO2,p}$ values ranging from 0.944 to 0.993 (average 0.98 ± 0.02) for the snow cover case (**Figure S2**). For the single-particle parameterization, $\gamma_{N2O5,p}$ values were 0.0048 and 0.0045 for the bare ground and snow case periods, respectively, with calculated $\Phi_{ClNO2,p}$ of 0.138 and 0.121, respectively. For both methods, both parameters were within the wide range ($\gamma_{N2O5,p}$: 10^{-4} – 0.1 and $\Phi_{ClNO2,p}$: 0-1) reported by previous laboratory and field studies.[68,69] However, the calculated $\gamma_{N2O5,p}$ and $\Phi_{ClNO2,p}$ values from the bulk method (Sc1) were roughly factors of 6-8 higher than the single-particle parameterization (Sc2), thus explaining the large difference in simulated $ClNO_2$ between the two scenarios. Notably, the differences in $\gamma_{N2O5,p}$ and $\Phi_{ClNO2,p}$ between the two methods are higher than in McNamara et al.,[35] who reported 2-3 times higher $\gamma_{N2O5,p}$ and $\Phi_{ClNO2,p}$ using the bulk method compared to the single-particle parameterization for wintertime Ann Arbor, MI.

Scenario 3 (Sc3) was constrained with observationally derived $ClNO_2$ surface flux, reported previously by McNamara et al.[27], in addition to $ClNO_2$ production from particles using the single-particle parameterization (Sc2). These fluxes describe $ClNO_2$ surface deposition to the bare ground and emission from the snow cover. When the observationally derived $ClNO_2$ flux was constrained in the model, the bare ground case simulation (**Figure 4a**, Sc3) further underestimated the observed $ClNO_2$ mole ratios and only explained on average 53 ± 12 % of the observed $ClNO_2$. Adjusting the simulation based on the uncertainty in the measurement-derived $ClNO_2$ deposition velocity did not make a significant difference. For the snow cover case (**Figure 4b**, Sc3), constraining the $ClNO_2$ surface flux from snow[27] resulted in lower $ClNO_2$ mole ratios (average 2 ± 1 times range 1-5 times) than observations during the night until 1:00 EST. Therefore, for the snow case, adding the snowpack $ClNO_2$ emission flux improved the $ClNO_2$ agreement compared to Sc2, which included only aerosol particle-produced $ClNO_2$. The large measurement uncertainties in the snowpack $ClNO_2$ emission fluxes resulted in a significant range of modeled $ClNO_2$ (**Figure 4b**), indicating that the $ClNO_2$ simulations were highly sensitive to the snowpack emissions. The important role of snowpack $ClNO_2$ production in the simulations is consistent with the whole-campaign observations by Kulju et al.,[28] who found higher $ClNO_2$ mole ratios when snow-covered ground was present, which could not be explained by air turbulence, N_2O_5, or several other variables, and attributed this finding to the snowpack $ClNO_2$ flux. The NO_2 level does not have a significant impact on the simulated ground level $ClNO_2$, as shown in **Figure S12**, since the corresponding model layer was constrained with the measured N_2O_5 at the field site.

The simulated $ClNO_2$ mole ratios were typically lower than observations for Sc2 and Sc3, which both used the single-particle parameterization (**Figure 4**). The weighted $\gamma_{N2O5,p}$ and $\Phi_{ClNO2,p}$ values depend on the laboratory-derived quantities chosen for each ambient particle type as summarized in **Table S3**. Therefore, uncertainties derive from limited laboratory studies of realistic particle types and matching these to the ambient particles. During the two case days, the majority of the particles, by number, corresponded to residential wood burning (**Figure S6**). To our knowledge, only one laboratory study has reported $\gamma_{N2O5,p}$ and $\Phi_{ClNO2,p}$ values for biomass burning aerosols.[105] Goldberger et al.[105] reported $\gamma_{N2O5,p}$ values ranging from 2×10^{-3} to 6×10^{-3} and $\Phi_{ClNO2,p}$ ranging from non-detectable to 50 % from burning various types of vegetation, depending on fuel chloride content. For the single particle parameterization, we applied the $\gamma_{N2O5,p}$ value from Goldberger et al.[105] for aerosols produced from burning longleaf pine needles (0.003). The $\Phi_{ClNO2,p}$ value from the same study for aerosols produced from burning saw palmetto (0.03) was used,[105] even though this fuel has a chloride content higher than expected for residential wood burning fuels in Michigan. As the modeled $ClNO_2$ from the single-particle parameterization (Sc2 and Sc3) underestimated the observations, the overall $ClNO_2$ yield was increased by a factor of 3 ($\Phi_{ClNO2,p} = 0.36$) for Sc4, which improved agreement with the observed $ClNO_2$ mole ratios (**Figure 4**). For the bare ground case, average $ClNO_2$ during the night was measured to be 22 ± 13 ppt, compared to 24 ± 10 ppt for Sc4. For the snow cover case, average $ClNO_2$ was measured to be 20 ± 5 ppt from sunset to 1:00, compared to 19 ± 6 ppt for Sc4. This is equivalent to increasing the $\Phi_{ClNO2,p}$ from biomass burning aerosols by ~10 times ($\Phi_{ClNO2,p} = \sim 0.3$). While this increased $\Phi_{ClNO2,p}$ was similar to previous field estimates of biomass burning influenced air masses ($\Phi_{ClNO2,p}$ of 0.06 – 0.2),[30] this is surprising as the chloride content of the particles was below the EDX detection limit, suggesting trace chloride levels. This low level of particulate chloride is expected for residential fuels likely to be dominated by wood with low chloride content. The $ClNO_2$ yield from biomass burning aerosols can be affected by various factors including organic coating and chloride content, which are impacted by the type of vegetation and aging during atmospheric transport.[105–107] Therefore, further laboratory studies deriving N_2O_5 uptake and $ClNO_2$ yield values with varying burn conditions and different types of vegetation are required to improve understanding and constraint of $ClNO_2$ production from biomass burning aerosols, especially residential wood burning aerosols.

3.4. Vertically-resolved $ClNO_2$ from aerosol particles and snow

While both aerosol particles and snow contribute to $ClNO_2$ formation (Sections 3.2 and 3.3), the relative contributions of each to the simulated vertical distributions of $ClNO_2$ were compared for the best model scenario (Sc4). To isolate the aerosol particle production only, a modified Sc4 simulation was run in which the snow $ClNO_2$ flux was not included (**Figure 5a**). This was compared to the simulation results of Sc4 with $ClNO_2$ production from both aerosol particles and surface snow, with the snow constrained by the measurement-derived flux **(Figure 5b)**. This scenario agrees best with the observations until 1:00 local time when measured $ClNO_2$ started declining due to atmospheric mixing (Section 3.1).

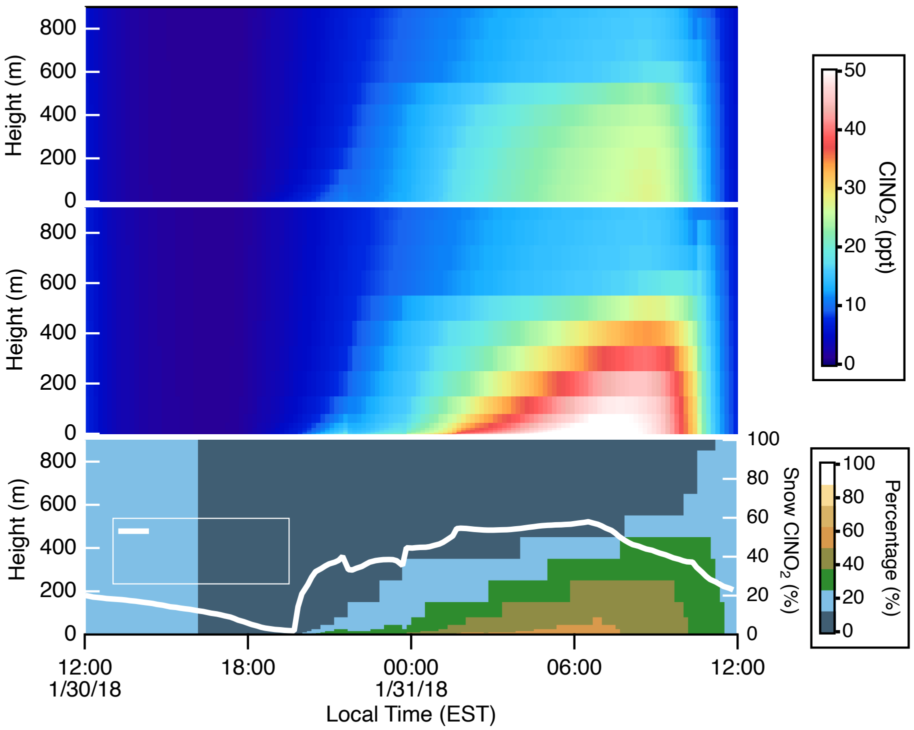

Figure 5 Vertical and diel distributions of simulated $ClNO_2$ mole ratios with formation from: (a) particles and (b) particles + snow emission. The $ClNO_2$ yield was multiplied by three for the single particle parameterization (model scenario Sc4 in Figure 4). Observationally driven $ClNO_2$ emission fluxes from snow, reported by McNamara et al. (2021), were used for snow emissions (see Figure 1). (c) Vertically resolved percentage of the modeled $ClNO_2$ from the difference between ***b*** (particles + snow) and ***a*** (particles) are shown as a function of time, with the percentage at ground level (1.4 m) from snow emissions. Nocturnal stable boundary layer height was estimated to be ~ 450 m (**Figure S10**).

For both aerosol only and aerosol + snow scenarios, modeled $ClNO_2$ in the nocturnal boundary layer steadily increased throughout the night. For the aerosol particle only simulations (Figure 5a) the highest levels were simulated to be at around 8:30 and ranged 23 – 27 ppt of $ClNO_2$ throughout the boundary layer. When both aerosol particles and surface snow were sources of $ClNO_2$ (**Figure 5b**), the maximum $ClNO_2$ levels reached 65 ppt at 6:30 for the lowest atmospheric model layer (i.e., the layer right above the snowpack). The maximum percentage of $ClNO_2$ from snow emissions (**Figure 5c**) was up to 61 % at 6:30 local time in the lowest atmospheric model layer. During the nighttime (sunset to 1 pm), the average contribution of snowpack-produced $ClNO_2$ was 36 ± 9 % (range 2 - 47 %) in the surface model layer corresponding to the observation height (1.4 m). It should be noted that the modeled turbulent transport is uncertain (supporting information, **S3**), and reduced model-measurement agreement was found after 1:00. However, despite uncertainties, it is clear that the saline snowpack can be a significant source of $ClNO_2$ in the wintertime urban environment.

4. Conclusion

In this study, we examined the contributions of $ClNO_2$ production from aerosol particles and the urban wintertime snowpack in Kalamazoo, MI, using an observationally constrained atmosphere and snow coupled 1D model. The modeling study was motivated by the work of McNamara et al.[27] who showed net $ClNO_2$ surface deposition over bare ground and net $ClNO_2$ emission over snow covered ground, with no significant difference in N_2O_5 deposition velocities. Kulju et al.[28] reported higher $ClNO_2$ levels over snow covered ground compared to bare ground across the entire field campaign. Therefore, two case periods, over bare ground and snow cover, were simulated to examine vertically-resolved contributions of $ClNO_2$ produced from aerosol particles and saline snow, both impacted by road salt application for deicing.

The model was constrained with snow parameters and surface observations, including observationally driven $ClNO_2$ surface flux reported by McNamara et al.[27] The snowpack $ClNO_2$ emission flux from the snow module was ~6 times higher than the measurement-derived flux. This overestimation of the snow module in simulating the observed surface $ClNO_2$ flux is due to the many model uncertainties, including the unknown availability of chloride in the snowpack for reaction, which is influenced by the physical characteristics of the snow grains. The chemical and physical complexity of the snowpack as a reactive media is yet to be fully represented in models.[102]

Further laboratory and field studies investigating the various factors controlling snow trace gas (including $ClNO_2$) production are needed.

When comparing different parameterization methods of $ClNO_2$ production from aerosol particles, model results show that assuming a homogenous aerosol composition (i.e. the "bulk" method)[35] overestimated the surface level measurements. This overestimation in simulated $ClNO_2$ when using the bulk method was also reported by McNamara et al.[27] for a previous wintertime study in Ann Arbor, MI. This demonstrates that the assumption of homogenous aerosol particle composition leads to an unrealistic representation of $ClNO_2$ production, since not all particles have equivalent N_2O_5 uptake values and not all particles contain chloride. However, model results of the single-particle (chemically-resolved surface area) parameterization explained only 30-40 % of the measured surface $ClNO_2$ for both case days. Including measurement-derived $ClNO_2$ emissions from surface snow improved agreement with measured ground level $ClNO_2$ for the snow case, underestimating by ~50 %. Model sensitivity studies showed that the observed $ClNO_2$ levels were within the model simulations, given the large uncertainty in the measurement-derived $ClNO_2$ emissions. Constraining the measured $ClNO_2$ surface deposition for the bare ground case further reduced the simulated $ClNO_2$. This result demonstrates the need for additional studies of $ClNO_2$ surface deposition velocities and comparison to results from numerical models. To improve the simulations for both case days, the overall single-particle parameterization $ClNO_2$ yield was increased by a factor of three, which led to agreement with the observations. However, limited information is available on the efficiency of $ClNO_2$ generation from authentic particle types, and more laboratory studies are needed to constrain the parametrization and reduce this uncertainty. In particular, there is high uncertainty from using N_2O_5 uptake and $ClNO_2$ yield values from only one study of biomass burning particles[105] from vegetation that are not representative of the field site.

The results in this study show the significant contribution of $ClNO_2$ production from an urban wintertime snowpack. The snowpack-emitted $ClNO_2$ was simulated to be vertically transported throughout the nocturnal stable boundary layer. Vertical profiles of modeled $ClNO_2$ show that the contribution of snowpack $ClNO_2$ can be up to ~60 % near the surface, decreasing to ~9 % near the top of the boundary layer. This highlights how reactions on the surface snowpack likely have a significant influence on atmospheric oxidation and composition upon $ClNO_2$ photolysis during the following day. Vertically-resolved observations are needed to improve understanding of $ClNO_2$ over the saline snowpack and enable further evaluation and quantitation of the vertically-resolved contributions of $ClNO_2$ production from aerosol particles and the saline snowpack. The results of this study can be extended to other saline snowpacks, such as coastal regions, where significant levels of chloride can accumulate in snow through sea salt aerosol deposition.[108]

Supporting Information

Further details on CIMS measurements (S1); 1D-model set-up (S2); turbulent transport calculations in model (S3); heterogeneous reactions on aerosols and snowpack (S4); CCSEM-EDX analysis of particles (S5); $ClNO_2$ model simulations in residual layer (S6); additional model constraints (Table S1); snow parameter inputs in model (Table S2); N_2O_5 uptakes and ClNO2 yields of different particle (Table S3); observed HCl (Figure S1); parameters used in calculating N_2O_5 uptake and $ClNO_2$ yield (Figure S2); particle number concentration and total surface area (Figure S3); size distributions of particles (Figure S4); SEM images and EDX spectra of particles (Figure S5); size distribution of particles from CCSEM-EDX (Figure S6); snow N_2O_5 uptake and $ClNO_2$ yield (Figure S7); diel friction velocity and eddy diffusivity (Figure S8); 1D model schematic (Figure S9); vertical absolute humidity, potential temperature, and eddy diffusivity

(Figure S10); estimated boundary layer height and eddy diffusivity (Figure S11); and modeled NO_2 (Figure S12).

Acknowledgements

Financial support was provided by the National Science Foundation (AGS-1738588 and PLR-1417914) and the University of Michigan (U-M) College of Literature, Science, and the Arts and Department of Chemistry. D.J. was supported by the National Center for Atmospheric Research Advanced Study Program for efforts during manuscript revisions. Q.C. was supported by the National Natural Science Foundation of China (42205115) during manuscript revisions. J.E. was supported by the Schweizerischer Nationalfonds zur Forderung der Wissenschaftlichen Forschung (155999). S.W. was partially supported by NOAA cooperative agreements NA17OAR4320101 and NA22OAR4320151. We thank Andrew Ault, Nicholas Ellsworth, and Matthew McNamara for assistance in preparing the mobile laboratory, Jasmine Mumpfield for snow ion chromatography analysis, Katheryn Kolesar for field campaign planning assistance, Angela Raso, Peter Peterson, Guy Burke, and Alexa Watson for fieldwork assistance, and James Brunemann for CCSEM-EDX data collection assistance. Steven B. Bertman and the Facilities Management Department at Western Michigan University are thanked for providing field site access and electrical support.

References

(1) Frenzel, A.; Scheer, V.; Sikorski, R.; George, Ch.; Behnke, W.; Zetzsch, C. Heterogeneous Interconversion Reactions of BrNO2, ClNO2, Br2, and Cl2. *J. Phys. Chem. A* **1998**, *102* (8), 1329–1337. https://doi.org/10.1021/jp973044b.

(2) George, Ch.; Behnke, W.; Scheer, V.; Zetzsch, C.; Magi, L.; Ponche, J. L.; Mirabel, Ph. Fate of ClNO2 Over Aqueous Solutions Containing Iodide. *Geophys Res Lett* **1995**, *22* (12), 1505. https://doi.org/10.1029/95GL01417.

(3) Madronich, S.; Flocke, S. Handbook of Environmental Chemistry. In *Handbook of Environmental Chemistry*; Springer_Verlag: Heidelberg, 1998; pp 1–26.

(4) Finlayson-Pitts, B. J.; M.J., E.; J.N., P. J. Formation of Chemically Active Chlorine Compounds by Reactions of Atmospheric NaCl Particles with Gaseous N2O5 and ClONO2. *Nature* **1989**, *337* (19).

(5) Asaf, D.; Tas, E.; Pedersen, D.; Peleg, M.; Luria, M. Long-Term Measurements of NO3 Radical at a Semiarid Urban Site: 2. Seasonal Trends and Loss Mechanisms. *Environ Sci Technol* **2010**, *44* (15), 5901–5907. https://doi.org/10.1021/es100967z.

(6) Dentener, F. J.; Crutzen, P. J. Reaction of N2O5 on Tropospheric Aerosols: Impact on the Global Distributions of NOx , O3 , and OH. *Journal of Geophysical Research: Atmospheres* **1993**, *98* (D4), 7149–7163. https://doi.org/10.1029/92JD02979.

(7) Hossaini, R.; Chipperfield, M. P.; Saiz-Lopez, A.; Fernandez, R.; Monks, S.; Feng, W.; Brauer, P.; Von Glasow, R. A Global Model of Tropospheric Chlorine Chemistry: Organic versus Inorganic Sources and Impact on Methane Oxidation. *J Geophys Res* **2016**, *121* (23), 14,271-14,297. https://doi.org/10.1002/2016JD025756.

(8) Horowitz, H. M.; Jacob, D. J.; Zhang, Y.; DIbble, T. S.; Slemr, F.; Amos, H. M.; Schmidt, J. A.; Corbitt, E. S.; Marais, E. A.; Sunderland, E. M. A New Mechanism for Atmospheric Mercury Redox Chemistry: Implications for the Global Mercury Budget. *Atmos Chem Phys* **2017**, *17* (10), 6353–6371. https://doi.org/10.5194/acp-17-6353-2017.

(9) Hoffmann, E. H.; Tilgner, A.; Schrödner, R.; Bräuer, P.; Wolke, R.; Herrmann, H. An Advanced Modeling Study on the Impacts and Atmospheric Implications of Multiphase Dimethyl Sulfide Chemistry. *Proc Natl Acad Sci U S A* **2016**, *113* (42), 11776–11781. https://doi.org/10.1073/pnas.1606320113.

(10) Cai, X.; Ziemba, L. D.; Griffin, R. J. Secondary Aerosol Formation from the Oxidation of Toluene by Chlorine Atoms. *Atmos Environ* **2008**, *42* (32), 7348–7359. https://doi.org/10.1016/j.atmosenv.2008.07.014.

(11) Riva, M.; Healy, R. M.; Flaud, P. M.; Perraudin, E.; Wenger, J. C.; Villenave, E. Gas- and Particle-Phase Products from the Chlorine-Initiated Oxidation of Polycyclic Aromatic Hydrocarbons. *Journal of Physical Chemistry A* **2015**, *119* (45), 11170–11181. https://doi.org/10.1021/acs.jpca.5b04610.

(12) Atkinson, R. Gas-Phase Tropospheric Chemistry of Volatile Organic Compounds: 1. Alkanes and Alkenes. *J Phys Chem Ref Data* **1997**, *26* (2), 215–290. https://doi.org/10.1063/1.556012.

(13) Levy, H. Normal Atmosphere: Large Radical and Formaldehyde Concentrations Predicted. *Science (1979)* **1971**, *173* (3992), 141–143. https://doi.org/10.1126/science.173.3992.141.

(14) Sherwen, T.; Evans, M. J.; Sommariva, R.; Hollis, L. D. J.; Ball, S. M.; Monks, P. S.; Reed, C.; Carpenter, L. J.; Lee, J. D.; Forster, G.; Bandy, B.; Reeves, C. E.; Bloss, W. J. Effects of Halogens on European Air-Quality. *Faraday Discuss* **2017**, *200*, 75–100. https://doi.org/10.1039/c7fd00026j.

(15) Li, Q.; Zhang, L.; Wang, T.; Tham, Y. J.; Ahmadov, R.; Xue, L.; Zhang, Q.; Zheng, J. Impacts of Heterogeneous Uptake of Dinitrogen Pentoxide and Chlorine Activation on Ozone and Reactive Nitrogen Partitioning: Improvement and Application of the WRF-Chem Model in Southern China. *Atmos Chem Phys* **2016**, *16* (23), 14875–14890. https://doi.org/10.5194/acp-16-14875-2016.

(16) Wang, X.; Jacob, D. J.; Eastham, S. D.; Sulprizio, M. P.; Zhu, L.; Chen, Q.; Alexander, B.; Sherwen, T.; Evans, M. J.; Lee, B. H.; Haskins, J. D.; Lopez-Hilfiker, F. D.; Thornton, J. A.; Huey, G. L.; Liao, H. The Role of Chlorine in Global Tropospheric Chemistry. *Atmos. Chem. Phys* **2019**, *19*, 3981–4003. https://doi.org/10.5194/acp-2018-1088.

(17) Sarwar, G.; Simon, H.; Xing, J.; Mathur, R. Importance of Tropospheric ClNO2 Chemistry across the Northern Hemisphere. *Geophys Res Lett* **2014**, *41* (11), 4050–4058. https://doi.org/10.1002/2014GL059962.

(18) Osthoff, H. D.; Roberts, J. M.; Ravishankara, A. R.; Williams, E. J.; Lerner, B. M.; Sommariva, R.; Bates, T. S.; Coffman, D.; Quinn, P. K.; Dibb, J. E.; Stark, H.; Burkholder, J. B.; Talukdar, R. K.; Meagher, J.; Fehsenfeld, F. C.; Brown, S. S. High Levels of Nitryl Chloride in the Polluted Subtropical Marine Boundary Layer. *Nat Geosci* **2008**, *1* (5), 324–328. https://doi.org/10.1038/ngeo177.

(19) Riedel, T. P.; Bertram, T. H.; Crisp, T. A.; Williams, E. J.; Lerner, B. M.; Vlasenko, A.; Li, S. M.; Gilman, J.; De Gouw, J.; Bon, D. M.; Wagner, N. L.; Brown, S. S.; Thornton, J. A. Nitryl Chloride and Molecular Chlorine in the Coastal Marine Boundary Layer. *Environ Sci Technol* **2012**, *46* (19), 10463–10470. https://doi.org/10.1021/es204632r.

(20) McNamara, S. M.; W. Raso, A. R.; Wang, S.; Thanekar, S.; Boone, E. J.; Kolesar, K. R.; Peterson, P. K.; Simpson, W. R.; Fuentes, J. D.; Shepson, P. B.; Pratt, K. A. Springtime Nitrogen Oxide-Influenced Chlorine Chemistry in the Coastal Arctic. *Environ Sci Technol* **2019**, *53* (14), 8057–8067. https://doi.org/10.1021/acs.est.9b01797.

(21) Thornton, J. A.; Kercher, J. P.; Riedel, T. P.; Wagner, N. L.; Cozic, J.; Holloway, J. S.; Dubé, W. P.; Wolfe, G. M.; Quinn, P. K.; Middlebrook, A. M.; Alexander, B.; Brown, S. S. A Large Atomic Chlorine Source Inferred from Mid-Continental Reactive Nitrogen Chemistry. *Nature* **2010**, *464* (7286), 271–274. https://doi.org/10.1038/nature08905.

(22) Mielke, L. H.; Furgeson, A.; Osthoff, H. D. Observation of ClNO2 in a Mid-Continental Urban Environment. *Environ Sci Technol* **2011**, *45*, 8889–8896. https://doi.org/10.1021/es201955u.

(23) Phillips, G. J.; Tang, M. J.; Thieser, J.; Brickwedde, B.; Schuster, G.; Bohn, B.; Lelieveld, J.; Crowley, J. N. Significant Concentrations of Nitryl Chloride Observed in Rural Continental Europe Associated with the Influence of Sea Salt Chloride and Anthropogenic Emissions. *Geophys Res Lett* **2012**, *39* (10), 1–5. https://doi.org/10.1029/2012GL051912.

(24) Yun, H.; Wang, T.; Wang, W.; Tham, Y. J.; Li, Q.; Wang, Z.; Poon, S. C. N. Nighttime NOx Loss and ClNO2 Formation in the Residual Layer of a Polluted Region: Insights from Field Measurements and an Iterative Box Model. *Science of the Total Environment* **2018**, *622–623* (x), 727–734. https://doi.org/10.1016/j.scitotenv.2017.11.352.

(25) Wang, X.; Wang, H.; Xue, L.; Wang, T.; Wang, L.; Gu, R.; Wang, W.; Tham, Y. J.; Wang, Z.; Yang, L.; Chen, J.; Wang, W. Observations of N2O5 and ClNO2 at a Polluted Urban Surface Site in North China: High N2O5 Uptake Coefficients and Low ClNO2 Product Yields. *Atmos Environ* **2017**, *156* (3), 125–134. https://doi.org/10.1016/j.atmosenv.2017.02.035.

(26) Wang, Z.; Wang, W.; Tham, Y. J.; Li, Q.; Wang, H.; Wen, L.; Wang, X.; Wang, T. Fast Heterogeneous N 2 O 5 Uptake and ClNO 2 Production in Power Plant and Industrial Plumes Observed in the Nocturnal Residual Layer over the North China Plain. *Atmos. Chem. Phys* **2017**, *175194* (3), 12361–12378. https://doi.org/10.5194/acp-17-12361-2017.

(27) McNamara, S. M.; Chen, Q.; Edebeli, J.; Kulju, K. D.; Mumpfield, J.; Fuentes, J. D.; Bertman, S. B.; Pratt, K. A. Observation of N2O5Deposition and ClNO2Production on the Saline Snowpack. *ACS Earth Space Chem* **2021**, *5* (5), 1020–1031. https://doi.org/10.1021/acsearthspacechem.0c00317.

(28) Kulju, K. D.; McNamara, S. M.; Chen, Q.; Kenagy, H. S.; Edebeli, J.; Fuentes, J. D.; Bertman, S. B.; Pratt, K. A. Urban Inland Wintertime N2O5 and ClNO2 Influenced by Snow-Covered Ground, Air Turbulence, and Precipitation. *Atmos Chem Phys* **2022**, *22* (4), 2553–2568. https://doi.org/10.5194/acp-22-2553-2022.

(29) Wagner, N. L.; Riedel, T. P.; Roberts, J. M.; Thornton, J. A.; Angevine, W. M.; Williams, E. J.; Lerner, B. M.; Vlasenko, A.; Li, S. M.; Dub??, W. P.; Coffman, D. J.; Bon, D. M.; De Gouw, J. A.; Kuster, W. C.; Gilman, J. B.; Brown, S. S. The Sea Breeze/Land Breeze Circulation in Los Angeles and Its Influence on Nitryl Chloride Production in This Region. *Journal of Geophysical Research Atmospheres* **2012**, *117* (22), 1–15. https://doi.org/10.1029/2012JD017810.

(30) Tham, Y. J.; Wang, Z.; Li, Q.; Wang, W.; Wang, X.; Lu, K.; Ma, N.; Yan, C.; Kecorius, S.; Wiedensohler, A.; Zhang, Y.; Wang, T. Heterogeneous N2O5 Uptake Coefficient and Production Yield of ClNO2 in Polluted Northern China: Roles of Aerosol Water Content and Chemical Composition. *Atmos Chem Phys* **2018**, *18* (17), 13155–13171. https://doi.org/10.5194/acp-18-13155-2018.

(31) Tham, Y. J.; Wang, Z.; Li, Q.; Yun, H.; Wang, W.; Wang, X.; Xue, L.; Lu, K.; Ma, N.; Bohn, B.; Li, X.; Kecorius, S.; Größ, J.; Shao, M.; Wiedensohler, A.; Zhang, Y.; Wang, T. Significant Concentrations of Nitryl Chloride Sustained in the Morning: Investigations of the Causes and Impacts on Ozone Production in a Polluted Region of Northern China. *Atmos Chem Phys* **2016**, *16* (23), 14959–14977. https://doi.org/10.5194/acp-16-14959-2016.

(32) Riedel, T. P.; Wagner, N. L.; Dubé, W. P.; Middlebrook, A. M.; Young, C. J.; Öztürk, F.; Bahreini, R.; Vandenboer, T. C.; Wolfe, D. E.; Williams, E. J.; Roberts, J. M.; Brown, S. S.; Thornton, J. A. Chlorine Activation within Urban or Power Plant Plumes: Vertically Resolved ClNO2 and Cl2 Measurements from a Tall Tower in a Polluted Continental Setting. *Journal of Geophysical Research Atmospheres* **2013**, *118* (15), 8702–8715. https://doi.org/10.1002/jgrd.50637.

(33) Mitroo, D.; Gill, T. E.; Haas, S.; Pratt, K. A.; Gaston, C. J. ClNO2 Production from N2O5 Uptake on Saline Playa Dusts: New Insights into Potential Inland Sources of ClNO2. *Environ Sci Technol* **2019**, *53* (13), 7442–7452. https://doi.org/10.1021/acs.est.9b01112.

(34) Royer, H. M.; Mitroo, D.; Hayes, S. M.; Haas, S. M.; Pratt, K. A.; Blackwelder, P. L.; Gill, T. E.; Gaston, C. J. The Role of Hydrates, Competing Chemical Constituents, and Surface Composition on ClNO2formation. *Environ Sci Technol* **2021**, *55* (5), 2869–2877. https://doi.org/10.1021/acs.est.0c06067.

(35) Mcnamara, S. M.; Kolesar, K. R.; Wang, S.; Kirpes, R. M.; May, N. W.; Gunsch, M. J.; Cook, R. D.; Fuentes, J. D.; Hornbrook, R. S.; Apel, E. C.; Laskin, A.; Pratt, K. A. Observation of Road Salt Aerosol Driving Inland Wintertime Atmospheric Chlorine

Chemistry. *ACS Cent. Sci.* **2020**, *6* (5), 684–694. https://doi.org/10.1021/acscentsci.9b00994.

(36) Owega, S.; Khan, B. U. Z.; D'Souza, R.; Evans, G. J.; Fila, M.; Jervis, R. E. Receptor Modeling of Toronto PM2.5 Characterized by Aerosol Laser Ablation Mass Spectrometry. *Environ Sci Technol* **2004**, *38* (21), 5712–5720. https://doi.org/10.1021/es035177i.

(37) Kumar, P.; Hopke, P. K.; Raja, S.; Casuccio, G.; Lersch, T. L.; West, R. R. Characterization and Heterogeneity of Coarse Particles across an Urban Area. *Atmos Environ* **2012**, *46*, 449–459. https://doi.org/10.1016/j.atmosenv.2011.09.018.

(38) Ault, A. P.; Peters, T. M.; Sawvel, E. J.; Casuccio, G. S.; Willis, R. D.; Norris, G. A.; Grassian, V. H. Single-Particle SEM-EDX Analysis of Iron-Containing Coarse Particulate Matter in an Urban Environment: Sources and Distribution of Iron within Cleveland, Ohio. *Environ Sci Technol* **2012**, *46* (8), 4331–4339. https://doi.org/10.1021/es204006k.

(39) Bari, M. A.; Kindzierski, W. B. Eight-Year (2007-2014) Trends in Ambient Fine Particulate Matter (PM2.5) and Its Chemical Components in the Capital Region of Alberta, Canada. *Environ Int* **2016**, *91*, 122–132. https://doi.org/10.1016/j.envint.2016.02.033.

(40) Wang, S.; McNamara, S. M.; Kolesar, K. R.; May, N. W.; Fuentes, J. D.; Cook, R. D.; Gunsch, M. J.; Mattson, C. N.; Hornbrook, R. S.; Apel, E. C.; Pratt, K. A. Urban Snowpack ClNO2Production and Fate: A One-Dimensional Modeling Study. *ACS Earth Space Chem* **2020**, *4* (7), 1140–1148. https://doi.org/10.1021/acsearthspacechem.0c00116.

(41) Mineral Commodity Summaries 2020. *United States Geological Survey* **2020**, 200.

(42) Kelly, V. R.; Findlay, S. E. G.; Schlesinger, W. H.; Menking, K.; Chatrchyan, A. M. *Road Salt: Moving Toward the Solution*; 2010.

(43) Kolesar, K. R.; Mattson, C. N.; Peterson, P. K.; May, N. W.; Prendergast, R. K.; Pratt, K. A. Increases in Wintertime PM2.5 Sodium and Chloride Linked to Snowfall and Road Salt Application. *Atmos Environ* **2018**, *177* (May 2017), 195–202. https://doi.org/10.1016/j.atmosenv.2018.01.008.

(44) Patra, A.; Colvile, R.; Arnold, S.; Bowen, E.; Shallcross, D.; Martin, D.; Price, C.; Tate, J.; ApSimon, H.; Robins, A. On Street Observations of Particulate Matter Movement and Dispersion Due to Traffic on an Urban Road. *Atmos Environ* **2008**, *42* (17), 3911–3926. https://doi.org/10.1016/j.atmosenv.2006.10.070.

(45) Mihailović, A.; Vučinić Vasić, M.; Ninkov, J.; Erić, S.; Ralević, N. M.; Nemeš, T.; Antić, A. Multivariate Analysis of the Contents of Metals in Urban Snow near Traffic Lanes in Novi Sad, Serbia. *Journal of the Serbian Chemical Society* **2014**, *79* (2), 265–276. https://doi.org/10.2298/JSC130311052M.

(46) Denby, B. R.; Ketzel, M.; Ellermann, T.; Stojiljkovic, A.; Kupiainen, K.; Niemi, J. V.; Norman, M.; Johansson, C.; Gustafsson, M.; Blomqvist, G.; Janhäll, S.; Sundvor, I. Road Salt Emissions: A Comparison of Measurements and Modelling Using the NORTRIP Road Dust Emission Model. *Atmos Environ* **2016**, *141*, 508–522. https://doi.org/10.1016/j.atmosenv.2016.07.027.

(47) Mielke, L. H.; Furgeson, A.; Odame-Ankrah, C. A.; Osthoff, H. D. Ubiquity of ClNO2 in the Urban Boundary Layer of Calgary, Alberta, Canada. *Can J Chem* **2016**, *94* (4), 414–423. https://doi.org/10.1139/cjc-2015-0426.

(48) Bartels-Rausch, T.; Jacobi, H. W.; Kahan, T. F.; Thomas, J. L.; Thomson, E. S.; Abbatt, J. P. D.; Ammann, M.; Blackford, J. R.; Bluhm, H.; Boxe, C.; Domine, F.; Frey, M. M.; Gladich, I.; Guzmán, M. I.; Heger, D.; Huthwelker, T.; Klán, P.; Kuhs, W. F.; Kuo, M. H.;

Maus, S.; Moussa, S. G.; McNeill, V. F.; Newberg, J. T.; Pettersson, J. B. C.; Roeselová, M.; Sodeau, J. R. A Review of Air-Ice Chemical and Physical Interactions (AICI): Liquids, Quasi-Liquids, and Solids in Snow. *Atmos Chem Phys* **2014**, *14* (3), 1587–1633. https://doi.org/10.5194/acp-14-1587-2014.

(49) Abbatt, J.; Thomas, J. L.; Abrahamsson, K.; Boxe, C.; Granfors, A.; Jones, A. E.; King, M. D.; Saiz-Lopez, A.; Shepson, P. B.; Sodeau, J.; Toohey, D. W.; Toubin, C.; Von Glasow, R.; Wren, S. N.; Yang, X. Halogen Activation via Interactions with Environmental Ice and Snow in the Polar Lower Troposphere and Other Regions. *Atmos Chem Phys* **2012**, *12* (14), 6237–6271. https://doi.org/10.5194/acp-12-6237-2012.

(50) Grannas, A. M.; Jones, A. E.; Dibb, J.; Ammann, M.; Anastasio, C.; Beine, H. J.; Bergin, M.; Bottenheim, J.; Boxe, C. S.; Carver, G.; Chen, G.; Crawford, J. H.; Dominé, F.; Frey, M. M.; Guzmán, M. I.; Heard, D. E.; Helmig, D.; Hoffmann, M. R.; Honrath, R. E.; Huey, L. G.; Hutterli, M.; Jacobi, H. W.; Klán, P.; Lefer, B.; McConnell, J.; Plane, J.; Sander, R.; Savarino, J.; Shepson, P. B.; Simpson, W. R.; Sodeau, J. R.; von Glasow, R.; Weller, R.; Wolff, E. W.; Zhu, T. An Overview of Snow Photochemistry: Evidence, Mechanisms and Impacts. *Atmos Chem Phys* **2007**, No. 7, 4329–4373. https://doi.org/10.5194/acpd-7-4165-2007.

(51) Abbatt, J. Interactions of Atmospheric Trace Gases with Ice Surfaces: Adsorption and Reaction. *Chem Rev* **2003**, *103* (12), 4783–4800. https://doi.org/10.1021/cr0206418.

(52) Domine, F.; Albert, M.; Huthwelker, T.; Jacobi, H. W.; Kokhanovsky, A. A.; Lehning, M.; Picard, G.; Simpson, W. R. Snow Physics as Relevant to Snow Photochemistry. *Atmos Chem Phys* **2008**, *8* (2), 171–208. https://doi.org/10.5194/acp-8-171-2008.

(53) Lopez-Hilfiker, F. D.; Constantin, K.; Kercher, J. P.; Thornton, J. A. Temperature Dependent Halogen Activation by N 2O 5 Reactions on Halide-Doped Ice Surfaces. *Atmos Chem Phys* **2012**, *12* (11), 5237–5247. https://doi.org/10.5194/acp-12-5237-2012.

(54) Halfacre, J. W.; Shepson, P. B.; Pratt, K. A. PH-Dependent Production of Molecular Chlorine, Bromine, and Iodine from Frozen Saline Surfaces. *Atmos Chem Phys* **2019**, *19* (7), 4917–4931. https://doi.org/10.5194/acp-19-4917-2019.

(55) Abbatt, J.; Oldridge, N.; Symington, A.; Chukalovskiy, V.; McWhinney, R. D.; Sjostedt, S.; Cox, R. A. Release of Gas-Phase Halogens by Photolytic Generation of OH in Frozen Halide-Nitrate Solutions: An Active Halogen Formation Mechanism? *Journal of Physical Chemistry A* **2010**, *114* (23), 6527–6533. https://doi.org/10.1021/jp102072t.

(56) Wren, S. N.; Donaldson, D. J.; Abbatt, J. P. D. Photochemical Chlorine and Bromine Activation from Artificial Saline Snow. *Atmos Chem Phys* **2013**, *13* (19), 9789–9800. https://doi.org/10.5194/acp-13-9789-2013.

(57) Pratt, K. A.; Custard, K. D.; Shepson, P. B.; Douglas, T. A.; Pöhler, D.; General, S.; Zielcke, J.; Simpson, W. R.; Platt, U.; Tanner, D. J.; Gregory Huey, L.; Carlsen, M.; Stirm, B. H. Photochemical Production of Molecular Bromine in Arctic Surface Snowpacks. *Nat Geosci* **2013**, *6* (5), 351–356. https://doi.org/10.1038/ngeo1779.

(58) Raso, A. R. W.; Custard, K. D.; May, N. W.; Tanner, D.; Newburn, M. K.; Walker, L.; Moore, R. J.; Huey, L. G.; Alexander, L.; Shepson, P. B.; Pratt, K. A. Active Molecular Iodine Photochemistry in the Arctic. *Proceedings of the National Academy of Sciences* **2017**, *114* (38), 10053–10058. https://doi.org/10.1073/pnas.1702803114.

(59) Wang, S.; McNamara, S. M.; Moore, C. W.; Obrist, D.; Steffen, A.; Shepson, P. B.; Staebler, R. M.; Raso, A. R. W.; Pratt, K. A. Direct Detection of Atmospheric Atomic

Bromine Leading to Mercury and Ozone Depletion. *Proc Natl Acad Sci U S A* **2019**, *116* (29), 14479–14484. https://doi.org/10.1073/pnas.1900613116.

(60) Custard, K. D.; Raso, A. R. W.; Shepson, P. B.; Staebler, R. M.; Pratt, K. A. Production and Release of Molecular Bromine and Chlorine from the Arctic Coastal Snowpack. *ACS Earth Space Chem* **2017**, *1* (3), 142–151. https://doi.org/10.1021/acsearthspacechem.7b00014.

(61) Apodaca, R. L.; Huff, D. M.; Simpson, W. R. The Role of Ice in N2O5 Heterogeneous Hydrolysis at High Latitudes. *Atmos Chem Phys* **2008**, *8* (24), 7451–7463. https://doi.org/10.5194/acp-8-7451-2008.

(62) Huff, D. M.; Joyce, P. L.; Fochesatto, G. J.; Simpson, W. R. Deposition of Dinitrogen Pentoxide, N2O5, to the Snowpack at High Latitudes. *Atmos Chem Phys* **2011**, *11* (10), 4929–4938. https://doi.org/10.5194/acp-11-4929-2011.

(63) Joyce, P. L.; Von Glasow, R.; Simpson, W. R. The Fate of NOx Emissions Due to Nocturnal Oxidation at High Latitudes: 1-D Simulations and Sensitivity Experiments. *Atmos Chem Phys* **2014**, *14* (14), 7601–7616. https://doi.org/10.5194/acp-14-7601-2014.

(64) Toyota, K.; McConnell, J. C.; Staebler, R. M.; Dastoor, A. P. Air-Snowpack Exchange of Bromine, Ozone and Mercury in the Springtime Arctic Simulated by the 1-D Model PHANTAS - Part 1: In-Snow Bromine Activation and Its Impact on Ozone. *Atmos Chem Phys* **2014**, *14* (8), 4101–4133. https://doi.org/10.5194/acp-14-4101-2014.

(65) Toyota, K.; Dastoor, A. P.; Ryzhkov, A. Air-Snowpack Exchange of Bromine, Ozone and Mercury in the Springtime Arctic Simulated by the 1-D Model PHANTAS - Part 2: Mercury and Its Speciation. *Atmos Chem Phys* **2014**, *14* (8), 4135–4167. https://doi.org/10.5194/acp-14-4135-2014.

(66) Thomas, J. L.; Stutz, J.; Lefer, B.; Huey, L. G.; Toyota, K.; Dibb, J. E.; Von Glasow, R. Modeling Chemistry in and above Snow at Summit, Greenland - Part 1: Model Description and Results. *Atmos Chem Phys* **2011**, *11* (10), 4899–4914. https://doi.org/10.5194/acp-11-4899-2011.

(67) Thomas, J. L.; Dibb, J. E.; Huey, L. G.; Liao, J.; Tanner, D.; Lefer, B.; Von Glasow, R.; Stutz, J. Modeling Chemistry in and above Snow at Summit, Greenland-Part 2: Impact of Snowpack Chemistry on the Oxidation Capacity of the Boundary Layer. *Atmos Chem Phys* **2012**, *12* (14), 6537–6554. https://doi.org/10.5194/acp-12-6537-2012.

(68) McDuffie, E. E.; Fibiger, D. L.; Dubé, W. P.; Lopez Hilfiker, F.; Lee, B. H.; Jaeglé, L.; Guo, H.; Weber, R. J.; Reeves, J. M.; Weinheimer, A. J.; Schroder, J. C.; Campuzano-Jost, P.; Jimenez, J. L.; Dibb, J. E.; Veres, P.; Ebben, C.; Sparks, T. L.; Wooldridge, P. J.; Cohen, R. C.; Campos, T.; Hall, S. R.; Ullmann, K.; Roberts, J. M.; Thornton, J. A.; Brown, S. S. ClNO2 Yields From Aircraft Measurements During the 2015 WINTER Campaign and Critical Evaluation of the Current Parameterization. *Journal of Geophysical Research: Atmospheres* **2018**, *123* (22), 12,994-13,015. https://doi.org/10.1029/2018JD029358.

(69) McDuffie, E. E.; Fibiger, D. L.; Dubé, W. P.; Lopez-Hilfiker, F.; Lee, B. H.; Thornton, J. A.; Shah, V.; Jaeglé, L.; Guo, H.; Weber, R. J.; Michael Reeves, J.; Weinheimer, A. J.; Schroder, J. C.; Campuzano-Jost, P.; Jimenez, J. L.; Dibb, J. E.; Veres, P.; Ebben, C.; Sparks, T. L.; Wooldridge, P. J.; Cohen, R. C.; Hornbrook, R. S.; Apel, E. C.; Campos, T.; Hall, S. R.; Ullmann, K.; Brown, S. S. Heterogeneous N_2O_5 Uptake during Winter: Aircraft Measurements during the 2015 WINTER Campaign and Critical Evaluation of

Current Parameterizations. *Journal of Geophysical Research: Atmospheres* **2018**, 4345–4372. https://doi.org/10.1002/2018JD028336.

(70) Staudt, S.; Gord, J. R.; Karimova, N. V.; McDuffie, E. E.; Brown, S. S.; Gerber, R. B.; Nathanson, G. M.; Bertram, T. H. Sulfate and Carboxylate Suppress the Formation of ClNO2 at Atmospheric Interfaces. *ACS Earth Space Chem* **2019**, *3* (9), 1987–1997. https://doi.org/10.1021/acsearthspacechem.9b00177.

(71) Gaston, C. J.; Thornton, J. A. Reacto-Diffusive Length of N2O5 in Aqueous Sulfate- and Chloride-Containing Aerosol Particles. *Journal of Physical Chemistry A* **2016**, *120* (7), 1039–1045. https://doi.org/10.1021/acs.jpca.5b11914.

(72) Bertram, T. H.; Thornton, J. A. Toward a General Parameterization of N2O5 Reactivity on Aqueous Particles: The Competing Effects of Particle Liquid Water, Nitrate and Chloride. *Atmos Chem Phys* **2009**, *9* (21), 8351–8363. https://doi.org/10.5194/acp-9-8351-2009.

(73) Behnke, W.; George, C.; Scheer, V.; Zetzsch, C. Production and Decay of ClNO2 from the Reaction of Gaseous N2O5 with NaCl Solution: Bulk and Aerosol Experiments. *Journal of Geophysical Research: Atmospheres* **1997**, *102* (D3), 3795–3804. https://doi.org/10.1029/96JD03057.

(74) Hallquist, M.; Stewart, D. J.; Stephenson, S. K.; Cox, R. A. Hydrolysis of N2O5 on Sub-Micron Sulfate Aerosols. *Physical Chemistry Chemical Physics* **2003**, *5* (16), 3453–3463. https://doi.org/10.1039/b301827j.

(75) Folkers, M.; Mentel, T. F.; Wahner, A. Influence of an Organic Coating on the Reactivity of Aqueous Aerosols Probed by the Heterogeneous Hydrolysis of N2O5. *Geophys Res Lett* **2003**, *30* (12), 2–5. https://doi.org/10.1029/2003GL017168.

(76) Anttila, T.; Kiendler-Scharr, A.; Mentel, T. F.; Tillmann, R. Size Dependent Partitioning of Organic Material: Evidence for the Formation of Organic Coatings on Aqueous Aerosols. *J Atmos Chem* **2007**, *57* (3), 215–237. https://doi.org/10.1007/s10874-007-9067-9.

(77) Cosman, L. M.; Knopf, D. A.; Bertram, A. K. N2O5 Reactive Uptake on Aqueous Sulfuric Acid Solutions Coated with Branched and Straight-Chain Insoluble Organic Surfactants. *Journal of Physical Chemistry A* **2008**, *112* (11), 2386–2396. https://doi.org/10.1021/jp710685r.

(78) Thornton, J. A.; Abbatt, J. P. D. N2O5 Reaction on Submicron Sea Salt Aerosol: Kinetics, Products, and the Effect of Surface Active Organics. *Journal of Physical Chemistry A* **2005**, *109* (44), 10004–10012. https://doi.org/10.1021/jp054183t.

(79) McNeill, V. F.; Patterson, J.; Wolfe, G. M.; Thornton, J. A. The Effect of Varying Levels of Surfactant on the Reactive Uptake of N2O5 to Aqueous Aerosol. *Atmos Chem Phys* **2006**, *6* (6), 1635–1644. https://doi.org/10.5194/acp-6-1635-2006.

(80) Gaston, C. J.; Thornton, J. A.; Ng, N. L. Reactive Uptake of N2O5 to Internally Mixed Inorganic and Organic Particles: The Role of Organic Carbon Oxidation State and Inferred Organic Phase Separations. *Atmos Chem Phys* **2014**, *14* (11), 5693–5707. https://doi.org/10.5194/acp-14-5693-2014.

(81) Thornton, J. A.; Braban, C. F.; Abbatt, J. P. D. N2O5 Hydrolysis on Sub-Micron Organic Aerosols: The Effect of Relative Humidity, Particle Phase, and Particle Size. *Physical Chemistry Chemical Physics* **2003**, *5* (20), 4593. https://doi.org/10.1039/b307498f.

(82) Griffiths, P. T.; Cox, R. A. Temperature Dependence of Heterogeneous Uptake of N2O5 by Ammonium Sulfate Aerosol. *Atmospheric Science Letters* **2009**, *10*, 159–163. https://doi.org/10.1002/asl.225.

(83) Brown, S. S.; Dubé, W. P.; Fuchs, H.; Ryerson, T. B.; Wollny, A. G.; Brock, C. A.; Bahreini, R.; Middlebrook, A. M.; Neuman, T. A.; Atlas, E.; Roberts, J. M.; Osthoff, H. D.; Trainer, M.; Fehsenfeld, F. C.; Ravishankara, A. R. Reactive Uptake Coefficients for N2O5 Determined from Aircraft Measurements during the Second Texas Air Quality Study: Comparison to Current Model Parameterizations. *Journal of Geophysical Research Atmospheres* **2009**, *114* (11), 1–16. https://doi.org/10.1029/2008JD011679.

(84) Chang, W. L.; Brown, S. S.; Stutz, J.; Middlebrook, A. M.; R., B.; Wagner, N. L.; Dub\'e, W. P.; Pollack, I. B.; Ryerson, T. B.; Riemer, N. Evaluating N2O5 Heterogeneous Hydrolysis Parameterizations for CalNex 2010. *J. Geophys. Res.* **2016**, *121*, 5051–5070. https://doi.org/10.1002/2015JD024737.Nighttime.

(85) Phillips, G. J.; Thieser, J.; Tang, M.; Sobanski, N.; Schuster, G.; Fachinger, J.; Drewnick, F.; Borrmann, S.; Bingemer, H.; Lelieveld, J.; Crowley, J. N. Estimating N2O5 Uptake Coefficients Using Ambient Measurements of NO3, N2O5, ClNO2 and Particle-Phase Nitrate. *Atmos Chem Phys* **2016**, *16* (20), 13231–13249. https://doi.org/10.5194/acp-16-13231-2016.

(86) Wagner, N. L.; Riedel, T. P.; Young, C. J.; Bahreini, R.; Brock, C. A.; Dubé, W. P.; Kim, S.; Middlebrook, A. M.; Öztürk, F.; Roberts, J. M.; Russo, R.; Sive, B.; Swarthout, R.; Thornton, J. A.; VandenBoer, T. C.; Zhou, Y.; Brown, S. S. N 2 O 5 Uptake Coefficients and Nocturnal NO 2 Removal Rates Determined from Ambient Wintertime Measurements. *Journal of Geophysical Research: Atmospheres* **2013**, *118* (16), 9331–9350. https://doi.org/10.1002/jgrd.50653.

(87) McDuffie, E. E.; Edwards, P. M.; Gilman, J. B.; Lerner, B. M.; Dubé, W. P.; Trainer, M.; Wolfe, D. E.; Angevine, W. M.; DeGouw, J.; Williams, E. J.; Tevlin, A. G.; Murphy, J. G.; Fischer, E. v.; McKeen, S.; Ryerson, T. B.; Peischl, J.; Holloway, J. S.; Aikin, K.; Langford, A. O.; Senff, C. J.; Alvarez, R. J.; Hall, S. R.; Ullmann, K.; Lantz, K. O.; Brown, S. S. Influence of Oil and Gas Emissions on Summertime Ozone in the Colorado Northern Front Range. *J Geophys Res* **2016**, *121* (14), 8712–8729. https://doi.org/10.1002/2016JD025265.

(88) Hanson, D. R.; Ravishankara, A. R. The Reaction Probabilities of ClONO2 and N2O5 on Polar Stratospheric Cloud Materials. *J Geophys Res* **1991**, *96* (D3), 5081–5090. https://doi.org/10.1029/90JD02613.

(89) George, C.; Ponche, J. L.; Mirabel, P.; Behnke, W.; Scheer, V.; Zetzsch, C. Study of the Uptake of N2O5 by Water and NaCl Solutions. *Journal of Physical Chemistry* **1994**, *98* (35), 8780–8784. https://doi.org/10.1021/j100086a031.

(90) Davis, J. M.; Bhave, P. V.; Foley, K. M. Parameterization of N2O5 Reaction Probabilities on the Surface of Particles Containing Ammonium, Sulfate, and Nitrate. *Atmos Chem Phys* **2008**, *8* (17), 5295–5311. https://doi.org/10.5194/acp-8-5295-2008.

(91) Liao, J.; Sihler, H.; Huey, L. G.; Neuman, J. A.; Tanner, D. J.; Friess, U.; Platt, U.; Flocke, F. M.; Orlando, J. J.; Shepson, P. B.; Beine, H. J.; Weinheimer, A. J.; Sjostedt, S. J.; Nowak, J. B.; Knapp, D. J.; Staebler, R. M.; Zheng, W.; Sander, R.; Hall, S. R.; Ullmann, K. A Comparison of Arctic BrO Measurements by Chemical Ionization Mass Spectrometry and Long Path-Differential Optical Absorption Spectroscopy. *Journal of*

Geophysical Research Atmospheres **2011**, *116* (1), 1–14. https://doi.org/10.1029/2010JD014788.

(92) Kercher, J. P.; Riedel, T. P.; Thornton, J. A. Chlorine Activation by N2O5: Simultaneous, in Situ Detection of ClNO2 and N2O5 by Chemical Ionization Mass Spectrometry. *Atmos Meas Tech* **2009**, *2* (1), 193–204. https://doi.org/10.5194/amt-2-193-2009.

(93) Markovic, M. Z.; VandenBoer, T. C.; Baker, K. R.; Kelly, J. T.; Murphy, J. G. Measurements and Modeling of the Inorganic Chemical Composition of Fine Particulate Matter and Associated Precursor Gases in California's San Joaquin Valley during CalNex 2010. *Journal of Geophysical Research (Atmospheres)* **2014**, *119* (10), 6853–6866. https://doi.org/10.1002/2013JD021408.

(94) Markovic, M. Z.; Vandenboer, T. C.; Murphy, J. G. Characterization and Optimization of an Online System for the Simultaneous Measurement of Atmospheric Water-Soluble Constituents in the Gas and Particle Phases. *Journal of Environmental Monitoring* **2012**, *14* (7), 1872–1884. https://doi.org/10.1039/c2em00004k.

(95) Chen, Q.; Edebeli, J.; McNamara, S. M.; Kulju, K. D.; May, N. W.; Bertman, S. B.; Thanekar, S.; Fuentes, J. D.; Pratt, K. A. HONO, Particulate Nitrite, and Snow Nitrite at a Midlatitude Urban Site during Wintertime. *ACS Earth Space Chem* **2019**, *3* (5), 811–822. https://doi.org/10.1021/acsearthspacechem.9b00023.

(96) Khlystov, A.; Stanier, C.; Pandis, S. N. An Algorithm for Combining Electrical Mobility and Aerodynamic Size Distributions Data When Measuring Ambient Aerosol. *Aerosol Science and Technology* **2004**, *38* (SUPPL. 1), 229–238. https://doi.org/10.1080/02786820390229543.

(97) Madronich Sasha and Flocke, S. Theoretical Estimation of Biologically Effective UV Radiation at the Earth's Surface. In *Solar Ultraviolet Radiation*; Zerefos Christos S. and Bais, A. F., Ed.; Springer Berlin Heidelberg: Berlin, Heidelberg, 1997; pp 23–48.

(98) Cho, H.; Shepson, P. B.; Barrie, L. A.; Cowin, J. P.; Zaveri, R. NMR Investigation of the Quasi-Brine Layer in Ice/Brine Mixtures. *Journal of Physical Chemistry B* **2002**, *106* (43), 11226–11232. https://doi.org/10.1021/jp020449+.

(99) Jeong, D.; Seco, R.; Gu, D.; Lee, Y.; Nault, B. A.; Knote, C. J.; Mcgee, T.; Sullivan, J. T.; Jimenez, J. L.; Campuzano-Jost, P.; Blake, D. R.; Sanchez, D.; Guenther, A. B.; Tanner, D.; Gregory Huey, L.; Long, R.; Anderson, B. E.; Hall, S. R.; Ullmann, K.; Shin, H.-J.; Herndon, S. C.; Lee, Y.; Kim, D.; Ahn, J.; Kim, S. Integration of Airborne and Ground Observations of Nitryl Chloride in the Seoul Metropolitan Area and the Implications on Regional Oxidation Capacity during KORUS-AQ 2016. *Atmos Chem Phys* **2019**, *19* (19). https://doi.org/10.5194/acp-19-12779-2019.

(100) Sicard, P.; Paoletti, E.; Agathokleous, E.; Araminienė, V.; Proietti, C.; Coulibaly, F.; De Marco, A. Ozone Weekend Effect in Cities: Deep Insights for Urban Air Pollution Control. *Environ Res* **2020**, *191* (July). https://doi.org/10.1016/j.envres.2020.110193.

(101) Osthoff, H. D.; Odame-ankrah, C. A.; Tokarek, T. W.; Taha, Y. M.; Corinne, L. Low Levels of Nitryl Chloride in the Lower Fraser Valley of British Columbia. *Atmos Chem Phys* **2018**, *18*, 6293–6315.

(102) Domine, F.; Bock, J.; Voisin, D.; Donaldson, D. J. Can We Model Snow Photochemistry? Problems with the Current Approaches. *Journal of Physical Chemistry A* **2013**, *117* (23), 4733–4749. https://doi.org/10.1021/jp3123314.

(103) Malley, P. P. A.; Chakraborty, S.; Kahan, T. F. Physical Characterization of Frozen Saltwater Solutions Using Raman Microscopy. *ACS Earth Space Chem* **2018**, *2* (7), 702–710. https://doi.org/10.1021/acsearthspacechem.8b00045.

(104) Chakraborty, S.; Kahan, T. F. Physical Characterization of Frozen Aqueous Solutions Containing Sodium Chloride and Humic Acid at Environmentally Relevant Temperatures. *ACS Earth Space Chem* **2020**, *4* (2), 305–310. https://doi.org/10.1021/acsearthspacechem.9b00319.

(105) Goldberger, L. A.; Jahl, L. G.; Thornton, J. A.; Sullivan, R. C. N2O5 Reactive Uptake Kinetics and Chlorine Activation on Authentic Biomass-Burning Aerosol. *Environ Sci Process Impacts* **2019**, *21* (10), 1684–1698. https://doi.org/10.1039/c9em00330d.

(106) Ahern, A.; Goldberger, L.; Jahl, L.; Thornton, J.; Sullivan, R. C. Production of N2O5 and ClNO2 through Nocturnal Processing of Biomass-Burning Aerosol. *Environ Sci Technol* **2017**, acs.est.7b04386. https://doi.org/10.1021/acs.est.7b04386.

(107) Ahern, A. T.; Robinson, E. S.; Tkacik, D. S.; Saleh, R.; Hatch, L. E.; Barsanti, K. C.; Stockwell, C. E.; Yokelson, R. J.; Presto, A. A.; Robinson, A. L.; Sullivan, R. C.; Donahue, N. M. Production of Secondary Organic Aerosol During Aging of Biomass Burning Smoke From Fresh Fuels and Its Relationship to VOC Precursors. *Journal of Geophysical Research: Atmospheres* **2019**, *124* (6), 3583–3606. https://doi.org/10.1029/2018JD029068.

(108) Domine, F.; Sparapani, R.; Ianniello, A.; Beine, H. J. The Origin of Sea Salt in Snow on Arctic Sea Ice and in Coastal Regions. *Atmos. Chem. Phys* **2004**, *4*, 2259–2271.